Title

Inflammatory Cytokine TNFα Promotes the Long-Term Expansion of Primary Hepatocytes in 3D Culture

Journal

Cell, 175(6)

ISSN

0092-8674

Authors

Peng, Weng Chuan
Logan, Catriona Y
Fish, Matt
et al.

Publication Date

2018-11-01

DOI

10.1016/j.cell.2018.11.012

Peer reviewed

HHS Public Access

Author manuscript

Cell. Author manuscript; available in PMC 2019 May 02.

Published in final edited form as:

Cell. 2018 November 29; 175(6): 1607–1619.e15. doi:10.1016/j.cell.2018.11.012.

Tissue Repair Signals and *In Vitro* Culture: Inflammatory Cytokine TNFα Promotes the Expansion of Primary Hepatocytes in 3D Culture

Weng Chuan Peng[1], **Catriona Logan**[1], **Matt Fish**[1], **Teni Anbarchian**[1], **Francis Aguisanda**[1], **Adrian Alvarez**[1], **Peng Wu**[1,3], **Yinhua Jin**[1], **Junjie Zhu**[4], **Bin Li**[5], **Markus Grompe**[5], **Bruce Wang**[2], and **Roel Nusse**[1]

[1]Department of Developmental Biology, Howard Hughes Medical Institute, Stanford Institute for Stem Cell Biology and Regenerative Medicine, Stanford University School of Medicine, Stanford, CA 94305, USA.

[2]Department of Medicine and Liver Center, University of California San Francisco, San Francisco, CA 94143, USA.

[3]Department of Pediatrics, Stanford University School of Medicine, Stanford, CA 94305, USA.

[4]Department of Electrical Engineering, Stanford University, Stanford, CA 94305, USA.

[5]Oregon Stem Cell Center, Oregon Health and Science University, Portland OR 97239, USA.

SUMMARY

In the healthy adult liver, most hepatocytes proliferate minimally. Yet upon physical or chemical injury to the liver, hepatocytes intensely proliferate *in vivo* under the direction of multiple extracellular cues, including Wnt and pro-inflammatory signals. Currently, liver organoids can be readily generated *in vitro* from bile-duct epithelial cells, but not hepatocytes. Here we show that TNFα, an injury-induced inflammatory cytokine, promotes the expansion of hepatocytes in 3D culture and enables serial passaging and long-term culture for more than 6 months. Single-cell RNA sequencing reveals broad expression of hepatocyte markers. Strikingly, *in vitro*-expanded hepatocytes engrafted, and significantly repopulated, the injured livers of $Fah^{-/-}$ mice. We anticipate tissue repair signals can be harnessed to promote the expansion of otherwise hard-to-culture cell-types, with broad implications.

INTRODUCTION

The capacity to stably expand healthy, non-transformed cell-types *in vitro* would abundantly supply cells for regenerative therapies and provide ample material for basic biological

Corresponding author: Roel Nusse (rnusse@stanford.edu).

CONTRIBUTIONS

Conceptualization, W.C.P. and R.N.; Methodology, W.C.P; Investigation, W.C.P, C.L., M.F, F.A., A.A., T.A., J.Z., P.W., Y.J. and B.L. and B.W.; Writing – Original Draft, W.C.P., C.L. and R.N.; Funding Acquisition, M.G. and R.N.; Resources, M.G. and R.N.; Supervision, R.N.

Lead contact: Roel Nusse (rnusse@stanford.edu)

DECLARATION OF INTERESTS

The authors declare no competing interests.

studies. However, it is generally accepted that the majority of adult primary cell-types are refractory to *in vitro* expansion, perhaps because they divide infrequently *in vivo*. For example the liver—the focus of this study—is generally subject to a low turnover rate during homeostasis (Magami et al., 2002). The liver parenchyma comprises two major cell types: hepatocytes (~80 %) and bile-duct epithelial cells (BEC, ~20 %). BECs are responsible for bile-acid transport whereas hepatocytes execute varied functions including metabolism, detoxification, and protein production (Halpern et al., 2017; Miyajima et al., 2014). Moreover, hepatocytes are diverse and their function and gene expression differs depending on their location within the liver lobule (the functional unit of the liver), which is organized along a spatial axis spanning from the central vein (CV) to the portal vein (PV) (Kietzmann, 2017). Along the CV-PV axis, hepatocytes are heterogeneous: *Axin2*$^{+}$ pericentral hepatocytes residing next to the CV express various cytochrome enzymes and proliferate during homeostasis, ultimately replacing ~20-30% of hepatocytes across the lobule over 1 year, as shown by lineage tracing (Wang et al., 2015). They divide under the influence of WNT/RSPO3 signals secreted by CV endothelial cells (Wang et al., 2015). Separately, rare *Telomerase-expressing* hepatocytes scattered throughout the liver lobule also proliferate and generate small clones after long-term lineage tracing (Lin et al., 2018). However, taken as a whole, hepatocytes generally renew themselves slowly by comparison to fast-cycling tissues such as the small intestines, which renews itself every 3-5 days (Clevers et al., 2014).

In contrast to the resting liver, hepatocyte proliferation increases dramatically after physical or chemical damage. A trademark of the liver is its capacity to regenerate following injury: even after surgical removal of two-thirds of its mass (partial hepatectomy [PH]) it can regenerate to its original size in 5-7 days (Michalopoulos and DeFrances, 1997). The usually-quiescent mature hepatocytes enter an intense phase of DNA synthesis under the direction of injury-invoked regenerative signals that have been well documented (Kang et al., 2012; Michalopoulos, 2007). For instance, Kupffer cells (liver-resident macrophages) secrete inflammatory cytokines such as Interleukin (IL)-6 and Tumor Necrosis Factor (TNF)-α, which are crucial early signals that initiate regeneration (Michalopoulos, 2007). Plasma levels of Hepatocyte Growth Factor (HGF) and Epidermal Growth Factor (EGF) increase quickly following PH, functioning as potent mitogenic factors that stimulate DNA synthesis in hepatocytes (Lindroos et al., 1991; Skov Olsen et al., 1988). In addition, hepatocytes themselves secrete growth factors required for angiogenesis that include VEGF, FGF1 and TGFα (Michalopoulos, 2007). Non-parenchymal cells, such as stellate cells and endothelial cells, also contribute to liver regeneration. For example, stellate cells secrete HGF and norepinephrine, while endothelial cells secrete HGF and Heparin Binding-EGF (Michalopoulos, 2007). Corroborating the importance of these pro-inflammatory signals in liver regeneration, TNFR1 (TNF Receptor 1) and IL-6 knockout mice show impaired DNA synthesis after PH (Cressman et al., 1996; Yamada et al., 1997), and blocking TNFα with antibodies inhibits liver regeneration after PH (Akerman et al., 1992). Collectively, these studies demonstrate that inflammatory cytokines and growth factors are critical for tissue regeneration and restoration of liver functions.

The liver is not the only organ that relies on inflammatory signals for regeneration after injury. Indeed, inflammation and regeneration are closely linked across multiple tissues such as the skeletal muscle, intestine, colon, hair follicles, skin, and central nervous system

(Aurora and Olson, 2014; Karin and Clevers, 2016). The inflammatory cytokines IL-6, TNFα and their related family members activate a series of transcription factors that include NF-κB, JAK/Stat, AP-1 and YAP (Karin and Clevers, 2016). These inflammatory signals in turn enhance cellular proliferation by promoting cell-cycle entry (Karin and Clevers, 2016). In particular, excessive activation of NF-κB signaling is linked to tumor initiation in the intestine and hepatocellular carcinoma in the liver, suggestive of a more general role in cell cycle regulation (Karin and Greten, 2005; Oguma et al., 2008; Pikarsky et al., 2004; Schwitalla et al., 2013). Such observations led us to postulate that regenerative cytokines could be harnessed beyond the context of injury to expand otherwise hard-to-expand primary cell-types *in vitro*.

It has been challenging to culture and stably expand hepatocytes. Currently, liver organoids can only be generated from bile-duct epithelial cells (BEC) and “tumoroids” that are formed from primary liver cancer cells (Broutier et al., 2016; 2017; Huch et al., 2013; 2015). Signals that are widely-employed in prevailing organoid methods (Huch and Koo, 2015) or 2D culture (Katsuda et al., 2016) fail to expand primary hepatocytes in 3D culture. Given the role of inflammatory cytokines in tissue repair, we asked if such signals could be employed to expand hepatocytes *in vitro*. Here we find that the inflammatory signal TNFα enables the *in vitro* expansion of primary mouse hepatocytes in 3D culture, which broadly express markers of hepatocytes but not other cell-types, as revealed by single-cell RNA sequencing. Importantly, cultured hepatocytes can engraft the injured livers of $Fah^{-/-}$ mice, and robustly regenerate liver tissue *in vivo*.

RESULTS

TNFα promotes the expansion of primary hepatocytes in 3D culture

We first attempted to culture hepatocytes in 3D Matrigel droplets overlaid by culture media supplemented with EGF, HGF and the WNT agonist CHIR99021 (see Experimental Procedures). However, only a few colonies were observed after two weeks in culture (Figure 1A, 1B). Lipid droplets, which are frequently associated with cellular stress and impaired regeneration (Lee et al., 2015; Michalopoulos, 2007; Torbenson et al., 2002), were detected in many hepatocytes (Figure S1A). Most cells eventually deteriorated within the first two to three weeks of culture or after the first passage (Figure 1C).

TNFα is a pro-inflammatory signal critical for fetal liver growth and liver regeneration after injury (Beg et al., 1995; Kirillova et al., 1999; Yamada et al., 1997). We asked if TNFα could be used to expand hepatocytes *in vitro*. Strikingly, in the presence of TNFα, hepatocyte colony formation was observed in the first two weeks of culture, with colony-forming efficiencies of up to 15 % (i.e., 150 colonies formed per 1000 primary hepatocytes seeded; Figure 1A, 1B). The colonies were mostly comprised of cells with a single large nucleus with scant cytoplasm and some colonies were more than 100 μm in size (Figure S1B). To test if TNFα was continuously required for both the initiation as well as maintenance of colonies, TNFα was removed from the culture media after passaging (Figure 1C). We used Hoechst intensity as a measure of colony expansion. When TNFα was withdrawn after passaging, colonies showed a minimal increase in DNA content when compared to culture with TNFα (Figure 1D); accumulated lipid droplets massively, which

were visible under phase contrast or by LipidTOX staining; and many colonies eventually deteriorated in culture (Figure 1C, S1C). When TNFα was withdrawn at later passages, a similar outcome was observed (Figure 1D, S1D).

TNFα has been shown to induce DNA replication in hepatocytes through NF-κB signaling (Kirillova et al., 1999; Webber et al., 1998). To test if NF-κB signaling is required for the expansion of hepatocyte culture, we blocked NF-κB signaling using the specific ATP-competitive IKK-β inhibitor ML120B. Indeed, blockade of NF-κB signaling reduced the number of organoids (Figure S1E). Finally, another inflammatory cytokine critical for liver regeneration, IL-6, did not replace the role of TNFα in hepatocyte expansion, with most cells deteriorating after the first three weeks in culture (Figure S1F). Taken together, TNFα-containing culture conditions consistently allowed for serial passaging and expansion of hepatocyte colonies for multiple months in a TNFα-dependent manner, with the longest culture currently at 8 months (Figure 1E, S1G).

Characterization of hepatocyte cultures

3D hepatocyte colonies derived in our culture media were morphologically distinct from liver organoids previously derived from BECs (Huch et al., 2013; 2015). In our hepatocyte colonies, polygonal cells were tightly packed in compact 3D structures, with larger colonies organized with pseudo-glandular rosettes with occasional lumen-like structures (Figure 2A, S2A). Immunofluorescence revealed broad expression of the general hepatocyte marker HNF4α, with $CD26^+$ bile canaliculi structures located centrally, reminiscent of structural polarity typically present in the liver lobule (Figure 2A). YAP and NF-κB, transcription factors important for liver regeneration after injury, were nuclearly localized (Su et al., 2015; Yimlamai et al., 2014). In addition, proliferation marker KI67 was detected and mitotic cells could be observed by Hoechst staining (Figure 2A, S2A).

During liver regeneration, progenitor markers are often transiently upregulated while differentiation-associated genes are downregulated (Karin and Clevers, 2016; Michalopoulos and DeFrances, 1997; Su et al., 2015). Quantitative PCR (q-PCR) revealed that cultured hepatocytes expressed genes associated with hepatocyte functions such as *Alb, Ttr, Tat* and *Fah*, albeit at levels slightly lower than in freshly isolated primary hepatocytes (Figure 2B, S2B, grey bars). Periportal genes such as *Cps1* and *Cyp2f2* were strongly down-regulated, presumably due to the Wnt activator present in the expansion medium, as Wnt is known to suppress periportal genes *in vivo* (Benhamouche et al., 2006; Planas-Paz et al., 2016; Rocha et al., 2015) (Figure 2B). Other cytochrome enzymes expressed in the pericentral zone, such as *Cyp1a2* and *Cyp3a11*, were also markedly reduced (Figure 2B).

Next, we tested if expression of hepatocyte functional genes could be induced in culture in the absence of TNFα and in the presence of factors that promote maturation, such as dexamethasone (Michalopoulos et al., 2003). We used two different strategies to separately induce expression of pericentral and periportal genes, as such genes are usually induced by mutually exclusive signals *in vivo*: Wnt signaling has been shown to promote pericentral, and inhibit periportal, gene expression, while Ras signaling promotes periportal gene expression (Benhamouche et al., 2006; Hailfinger et al., 2006; Halpern et al., 2017; Planas-Paz et al., 2016; Rocha et al., 2015). To induce periportal gene expression, cultured cells

were switched to induction media for 4 days, in which EGF and HGF were maintained in the media while CHIR and TNFα were withdrawn (Figure 2B, S2B). The expression of *Alb* increased to a level comparable to primary hepatocytes, and *Cps1* and *Cyp2f2* were strongly upregulated (Figure 2B). Separately, to promote the expression of pericentral genes, the Wnt agonist CHIR was maintained while EGF, HGF and TNFα were withdrawn from the media. In this setting, the expression levels of *Cyp1a2, Cyp3a11* and *Gck*were upregulated (Figure 2B).

Next, we performed functional assays to further characterize the 3D hepatocyte cultures. First, cultured hepatocytes secreted high levels of albumin proteins into the media, with higher levels of albumin detected in EGF- induction media than expansion media, consistent with qPCR data (Figure 3A). Second, hepatocytes cultured in EGF-media displayed higher levels of CYP3A11 (the ortholog of human CYP3A4) enzymatic activity than expansion media, and unexpectedly, also Wnt- induction media. (Figure 3A). In both assays, the trend is maintained in 3- to 7- month cultures, indicating that functional properties are retained in long-term culture. Third, cultured hepatocytes could uptake fluorescently-conjugated low-density lipoprotein (LDL) (Figure 3B). Fourth, the addition of fluorescein diacetate dye led to rapid uptake and accumulation in the bile canaliculi structures and lumens between cells (Figure 3C, S3A), reflecting functional bile canaliculi. Fifth, hepatocytes could store glycogen, as detected by Periodic Acid-Schiff (PAS) staining (Figure 3D). In addition, cultured hepatocytes could be genetically manipulated, as shown by lentiviral transduction of *GFP* (Figure 3E, S3B). Lastly, 3D hepatocytes could be co-cultured with human umbilical vein endothelial cells (HUVECs). 3D hepatocyte-HUVEC aggregates were observed two days after the initiation of co-culture, and larger aggregates could be observed two weeks later (Figure 3F, S3C).

Single cell transcriptome analysis reveals expression of hepatocyte, proliferation and regeneration markers

To evaluate the gene expression profile of, and heterogeneity among, single hepatocytes after *in vitro* expansion, we performed single-cell RNA sequencing using the high-throughput 10x Genomics Chromium droplet-based system (Zheng et al., 2017). We performed single-cell RNA-seq on 1192 hepatocytes (derived from one male and one female mice) and jointly analyzed these data by Principal Component Analysis (PCA). The top 10 PCs were used for clustering analysis (Butler et al., 2018) and the resulting clusters were visualized in t-distributed stochastic neighboring embedding (t-SNE) projections (Figure 4A).

Hepatocyte markers such as *Alb, Apoa1, Ttr, Serpina1c, Hnf4a, Fga, Fn1, Rbp4, Glul*and *Slc1a2* were broadly and heterogeneously expressed across the entire population of cultured hepatocytes (Figure 4A). Gene ontology (GO) analysis of the most abundantly-expressed genes revealed an enrichment of relevant functional categories, including cytolysis, lipoprotein particle remodeling, blood coagulation, retinol metabolic process, regulation of G1/S phase transition, and response to tumor necrosis factor (Figure S4). Crucially, canonical biliary markers such as *Epcam, Krt7, Krt19, Aqp1, Aqp4* and *Cldn7* were present at low levels or not detected (Figure 4C in red, and not shown). On the contrary, hepatocyte epithelial markers such as *Krt8, Krt18* and *Tjp1* (*Cd26*) were highly expressed in many cells

(Figure 4C in red, and not shown), suggesting that the vast majority of cultured cells are hepatocytes, without evidence for a distinct subset of non-hepatocyte cells.

Clustering analyses of the entire population of cultured hepatocytes (Figure 4A) revealed a subset of cells (259/1192 cells) that expressed proliferation markers such as *Mki67, Ccna2, Cdk1, Top2a* and *Cenpm* (Figure 4D, S4A). GO analysis of genes differentially expressed by this putative cluster of proliferating cells confirmed enrichment for terms such as mitosis, cell cycle regulation, chromosome segregation, remodeling and DNA replication (Figure S4B). We thus assigned this subset of cells as cycling hepatocytes. The distinction between cycling versus non-cycling cells was also clearly captured by PC2 (Figure 4A). Of note, cells from male and female samples were similarly represented in the cycling and non-cycling hepatocytes; a small subset of female hepatocytes also formed a distinct cluster from the remaining hepatocytes (Figure 4A).

A key question is whether *in vitro*-expanded hepatocytes transcriptionally resemble primary hepatocytes. To this end we conducted single-cell RNA-seq of 1233 hepatocytes freshly isolated from 3-month old mice (Figure 5A). Genes associated with inflammatory responses typically showed little to no expression in healthy hepatocytes but were detected in cultured hepatocytes (Figure S5A), such as acute phase proteins serum amyloid A3, *Saa3* (and *Saa1, Saa2*) and lipocalin 2 (*Lcn2*), Haptoglobin (*Hp*) and clusterin (*Clu*) (Figure 5B). Acute phase proteins are usually expressed during inflammation to promote clearance of pathogens, and to limit excessive inflammatory responses (Robinson et al., 2016). For instance, *Lcn2* has been shown to exert protective effect against cytokine-induced stress during acute liver injury (Borkham-Kamphorst et al., 2013; Hu et al., 2015). Further, cytokines and chemokines (*Ccl20, Cxcl1, Cxcl5, Ccl2*), many of which are induced by TNFα or interleukins, were highly expressed in culture but notably absent in primary hepatocytes (Figure 5B).

Next, we examine the expression of regenerative factors that have been previously described to be critical for liver regeneration after partial hepatectomy (Costa et al., 2003; Karin and Clevers, 2016; Michalopoulos, 2007; Su et al., 2015). Notably, transcription factors *Rela* (i.e., NF-κB p65 subunit), *Stat3, Yap1, Jun* and *Fos* (which form the AP-1 complex) and *Myc* were detected (Figure 5C). In addition, growth factors that are secreted by hepatocytes *in vivo* that promote proliferation such as *Igf2* and *TGFα* (Michalopoulos and DeFrances, 1997), and angiogenesis factor *Vegfa* (Shimizu et al., 2001a; 2005). These data suggest that the mechanisms driving the expansion of hepatocytes in 3D culture may mimic some aspects of *in vivo* liver regeneration after injury.

In the expansion media, many serum proteins that are normally expressed in high abundance in the liver are downregulated (Figure S5A), including apolipoproteins (*Apoa2, Apoc3, Apoc1*), serine protease inhibitor (*Serpin3k, Serpin1e*), major urinary protein (*Mup3, Mup20, Mup2*), as well as metabolic p450 cytochrome enzymes (*Cyp3a11, Cyp2e1*). We asked if hepatocyte functional genes could be upregulated in culture. To this end, we compared the gene expression of hepatocytes in expansion media with 1245 cells cultured in EGF- induction media (which lack Wnt signal and TNFα) for 4 days of culture. Indeed, upon treatment with EGF-induction media, many functional genes were promoted (Figure

S5B). Notably, *Cyp3a11* and *Alb* were expressed at levels comparable to primary hepatocytes. Other upregulated genes include apolipoproteins *Apoa2* (and related members *Apoc3, Apoc1, Apoh*), *Serpinc1, Mup20, Aldob, Khk* and *Bhmt* (Figure 5D). Concomitantly, the expression of ribosomal genes *Rps* and *Rpl*, which are usually high during period of rapid proliferation (Warner, 1999), were downregulated, along with *Saa3, Clu, Ccl2 and Cxcl5* (Figure S5B). We also noted the downregulation of regeneration-associated markers, which are now more correlated with the expression levels in primary hepatocytes (Figure 5C). Taken together, *in vitro*-expanded hepatocytes maintained their hepatocyte identity, and upon withdrawal of expansion and inflammatory signals, they upregulate suites of genes associated with hepatocyte metabolic functions.

In vitro expanded hepatocytes engraft *Fah*-deficient mice

As a measure of whether *in vitro*-expanded hepatocytes retained functional characteristics, we transplanted these cells into the $Fah^{-/-}$ mouse model of liver failure. These mice lack the tyrosine metabolic enzyme *fumarylacetoacetate hydrolase* (*Fah*) and thus model human type 1 tyrosinemia patients that analogously harbor *FAH* mutations (Azuma et al., 2007; Grompe et al., 1993). In $Fah^{-/-}$ mice, liver injury can be induced by withdrawal of hepato-protective drug NTBC. All hepatocyte samples for transplant experiments were transported overnight in suspension in the form of 3D colonies. We reasoned that 3D colonies might promote stability and survival of hepatocytes compared to a single-cell suspension. ~50,000 – 100,000 colonies were injected intrasplenically as previously described (Azuma et al., 2007). One mouse died 72 days post-transplantation while the remaining two mice were sacrificed at 103 days after transplant. Immunohistochemistry and immunofluorescence for FAH showed significant engraftment (up to 80 %) (Figure 6A), in contrast to the modest (~1 %) engraftment that was previously reported upon transplantation of BEC-derived organoids (Huch et al., 2013). FAH+ cells were observed around the CV, PV and midlobular regions and displayed heterogeneity in nuclear and cell size (Figure 6B).

HNF4α staining was detected in all FAH+ cells, as well as host cells (Figure 6C). Engrafted colony-derived cells around the central vein (CV) expressed pericentral genes such as GLT1, GS and CYP2E1 (Figure 6D-F). Notably, the expression of these markers was not detected in host cells (Figure 6D-F). Engrafted cells, regardless of their pericentral or periportal location stained for CPS1, whereas host cells expressed low levels of CPS1 (Figure 6G). Of note, engrafted FAH+ cells did not stain for SOX9 or KRT7/19, which mark biliary cells (Figure 6H, S6I), confirming that cultured cells retained hepatocyte identity after transplantation. In a second independent transplant experiment, we injected two mice with 50 – 100 times fewer cells than used in the first experiment (~1,000 colonies) and one with a single-cell suspension. The livers of transplanted mice were harvested 3 – 4 months after transplant for analysis. FAH+ cells were detected in all three mice, at up to 2 % repopulation (Figure S6A). FAH+ clones as large as 600 μm could be observed; they also expressed functional markers and the proliferation marker KI67 (Figure S6B- S6H).

Next, we asked whether engraftment of cultured hepatocytes and subsequent regeneration utilizes signals known to promote hepatocyte proliferation during homeostasis, such as the Wnt signaling pathway (Wang et al., 2015). To track Wnt responsiveness in engrafted cells,

we first generated 3D hepatocytes from *Axin2-rtTA;TetO-H2B:GFP* donor mice and transplanted the cells into $Fah^{-/-}$ mice. Two days before the recipient mice were sacrificed, doxycycline was added to drinking water to induce *Axin2* reporter activity (which tracks Wnt signaling and leads to GFP expression). As expected, hepatocytes around the CVs were GFP+, indicating that they were responding to Wnt signals (Figure S7A, S7B). In addition, GFP+ cells were found at the boundary of FAH+ clones (Figure 7A, S7A, S7B). In contrast to larger clones that had a clear GFP+ boundary, smaller clones displayed GFP+ cells that were scattered throughout (Figure S7B), suggesting that the FAH- boundary might be a source of Wnt signaling. Consistent with this, GFP+ cells expressed another progenitor marker and the Wnt target gene TBX3 (Figure 7B, S7A, S7B). TBX3 expression was highest at the clone boundary but was largely absent from the center of the FAH+ clones. Of note, TBX3 expression is also detected at a lower level in host cells, suggesting the presence of a Wnt source outside of FAH+ clones (Figure 7B, S7). KI67 staining revealed proliferation of GFP expressing cells at the FAH+ nodule boundary (Figure 7C). Some cells that were more centrally located within the engrafted nodules also displayed KI67 staining (Figure S6H).

To query which Wnt family member ligands might regulate the engraftment of the FAH+ cells, we performed in situ hybridization (ISH). *Wnt9b* and *Wnt2* are known to be preferentially expressed in CV endothelial cells with some expression extending into the lobules (Preziosi et al., 2018; Wang et al., 2015). Consistent with this, we observed *Wnt9b* and *Wnt2* expression in the endothelium of central veins residing in FAH- regions (Figure S7C). In addition, we examined expression of R-spondin family members, as they potentiate Wnt signals in many tissues (de Lau et al., 2014) and *Rspo3* is expressed by the CVs in the liver (Planas-Paz et al., 2016; Rocha et al., 2015). Strikingly, *Rspo3* was highly expressed by vascular structures in FAH- injury zones (Figure S7C), and especially around the periphery of FAH+ clones (Figure 7D). To identify the cell-type that expresses *Rspo3*, we performed double-in situ hybridization (ISH). We used *Cd31* (*Pecam1*) to identify endothelial cells and *Cd45* (*Ptprc*) to broadly mark infiltrating and resident immune cells. Double ISH revealed that *Rspo3* was expressed in *Cd31*+ endothelial cells but not in clusters of *Cd45*+ cells (Figure S7C).

Amongst various R-spondin family members, ISH also revealed that *Rspo1* was only found in the liver mesothelium, but two additional Rspo family members, *Rspo2* and *Rspo4* were found in the liver lobule (Figure S7C). Both *Rspo2* and *Rspo4* localized to dense clusters of cells that morphologically resembled immune cells. They were often found next to vascular structures nearby FAH+ clones and were distributed in a manner similar to the arrangement of *Cd45*+ cells in FAH- area (Figure S7C). We speculate that these small cells may be Kupffer cells, although we did not confirm this directly. Similarly, TNFα, known to be secreted by Kupffer cells (Michalopoulos and DeFrances, 1997; Pikarsky et al., 2004), was also found in FAH- livers, localized to dense clusters of cells similar in morphology to those that express *Rspo2* and *Rspo4* (Figure S7C). Taken together, our data indicate that 3D hepatocytes can engraft $FAH^{-/-}$ mice, whereupon they continue to express hepatocyte markers, and that cells at the FAH+ clone boundary expand in the presence of WNT-RSPO signals and a regenerative signal-rich environment.

DISCUSSION

The majority of hepatocytes have little proliferative activity in the healthy liver, perhaps explaining challenges in generating long-term cultures from hepatocytes and other difficult-to-expand primary cell-types. Our data show that the inflammatory cytokine TNFα enables the long-term culture of primary hepatocytes—which have historically been difficult to expand *in vitro*—while retaining their functionality and engraftment potential. In the absence of TNFα, hepatocyte cultures degenerated within the first 2-3 weeks. Withdrawing TNFα at any point from the culture reduced hepatocyte expansion and resulted in lipid droplet accumulation and eventually deterioration of cells in culture, indicating the continued dependence of the cultures on TNFα for growth. *In vitro*-expanded 3D hepatocytes, upon treatment with induction media, displayed a variety of functional activities, for instances, albumin secretion, CYP3A11 enzymatic activity, LDL uptake, glycogen storage and secretion into bile canaliculi, even after long-term expansion. Single-cell RNA-seq revealed broad expression of hepatocyte markers and crucially, the absence of many non-hepatocyte markers. Interestingly, hepatocytes in culture also expressed markers typically associated with liver regeneration and proliferation after partial hepatectomy, suggesting that perhaps the mechanism driving *in vitro* expansion mimics the *in vivo* regeneration process. Upon withdrawal of expansion signals (Wnt and TNFα), many functional genes could be further upregulated, with some genes expressed to levels comparable to primary hepatocytes.

Cultured hepatocytes engrafted the livers of $Fah^{-/-}$ mice and continued to proliferate *in vivo*, leading to significant liver reconstitution (with up to 80% of the host liver replaced by FAH+ hepatocytes). This is striking, as previous efforts to culture liver cells *in vitro* have led to modest to little engraftment (~1% in the case of BEC-derived organoids) (Huch et al., 2013). The signals driving the *in vivo* proliferation of transplanted hepatocytes remain to be determined, but may include inflammatory signals that drive regeneration in other types of injury models, such as partial hepatectomy (Michalopoulos and DeFrances, 1997; Michalopoulos, 2017). We noticed an elevated level of *Wnt/Rspo3* expression in the injury area, produced by endothelial cells, as well as *Rspo2, Rspo4*, and *Tnfa* produced by infiltrating or resident immune cells. Of note, *Wnt9b/Rspo3* produced by the CV induces the proliferation of pericentral hepatocytes during homeostasis (Wang et al., 2015). Indeed, various studies have shown that angiogenesis is a critical aspect for liver regeneration and function, *in vivo* (Shimizu et al., 2001b; 2005; Taniguchi et al., 2001) and potentially *in vitro* (Camp et al., 2017; Takebe et al., 2013). VEGF secreted by regenerating hepatocytes induces sinusoidal endothelial cell proliferation and neutralizing VEGF impairs the proliferation of endothelial cells as well as hepatocytes (Taniguchi et al., 2001). These observations suggest that the crosstalk between hepatocytes and endothelial cells, which serve as a major source of WNT-RSPO signals, is essential for liver regeneration.

To capture the complexities associated with such communication between diverse cell-types, 3D hepatocyte cultures could eventually provide a more physiologically relevant system to study basic liver biology, model disease, and assess responses to drugs. Indeed, it has been proposed that cells cultured in 3D matrices more closely resemble their *in vivo* counterparts when cultured in 2D monolayers (Edmondson et al., 2014). For instance, pluripotent stem

cell-derived hepatocytes have been aggregated with endothelial and mesenchymal cells to form a 'liver bud' (Takebe et al., 2014). Here, we showed that 3D hepatocytes derived from primary hepatocytes aggregated readily with HUVEC in culture, and this may in future allow the generation of vascularized mini-liver that could be potentially used for organ transplants. In addition, we demonstrated that 3D hepatocytes could be genetically manipulated by lentiviral infection, and therefore they may be amenable to other gene editing tools such as CRISPR for correction of faulty genes to treat liver diseases.

Our work, in conjunction with the growing body of evidence for a role of inflammatory cytokines in tissue repair and regeneration, has the potential for application to other organs and disease processes beyond the liver. Regenerative cytokines, such as IL-6, TNFα and their related family members, have been broadly implicated in wound repair and the healing of many tissue compartments such as the colon, intestine (Lindemans et al., 2015), gastric tissue (Oguma et al., 2008), hair follicles (Chen et al., 2015), fracture healing (Gerstenfeld et al., 2003), and remyelination by oligodendrocyte progenitors (Arnett et al., 2001). For instances, damaged hair follicles secrete CCl2 to recruit macrophages to the site of injury, which in turn secrete TNFα to activate hair follicle regeneration (Chen et al., 2015), while muscle regeneration is stimulated by myoblasts-secreted TNFα. In addition, IL-22 and IL-6 have been shown to enhance intestinal stem cell proliferation after injury and in *in vitro* culture (Jeffery et al., 2017; Lindemans et al., 2015). More recently, it has been reported that IFN-γ produced by immune cells during parasitic infection induces the expansion of intestinal stem cells with fetal-like phenotypes (Nusse et al., 2018). We propose that harnessing *in vivo* regenerative signals for the *in vitro* expansion of cells in culture may be a powerful approach for manipulating hard-to-expand primary cell-types, with a view to potential applications in regenerative medicine.

CONTACT FOR REAGENT AND RESOURCE SHARING

Further information and requests for resources and reagents should be directed to and will be fulfilled by the Lead Contact, Roel Nusse (rnusse@stanford.edu).

EXPERIMENTAL MODEL AND SUBJECT DETAILS

The Institutional Animal Care and Use Committee at Stanford University approved all animal methods and experiments. Wild type C57BL/6J mice, Axin2-CreERT2 (B6.129(Cg)-Axin2 *tm1(cre/ERT2)Rnu*/J) (van Amerongen et al., 2012), Rosa26-mT/mG (B6.129(Cg)-Gt(ROSA)26Sor *tm4(ACTB-tdTomato,-EGFp)Luo*/*J* (Muzumdar et al., 2007), Axin2-rtTA (B6.Cg-Tg(Axin2-rtTA2S*M2)7Cos/J and TetO-H2B-GFP (Tg(tetO-HIST1H2BJ/GFP)47Efu/J) (Yu et al., 2007) were obtained from The Jackson Laboratory (JAX). Axin2- CreERT2:Rosa26-mT/mG mice were derived by crossing male heterozygous Axin2-CreERT2 with homozygous female Rosa26-mT/mG mice. Axin2-rtTA:TetO-H2B-GFP mice were derived by crossing either male or female heterozygous Axin2-rtTA mice with heterozygous TetO-H2B-GFP mice. All mice were housed with a 12-h light/dark cycle with ad libitum access to water and normal chow.

QUANTIFICATION AND STATISTICAL ANALYSIS

Statistical comparisons in Figure 1D were carried out using the non-parametric Mann Whitney test, with the following significance: ns = $P > 0.05$, * = $P \leq 0.05$, ** = $P \leq 0.01$, *** = $P \leq 0.001$, **** = $P \leq 0.0001$

METHOD DETAILS

Hepatocyte isolation and culture

Hepatocytes were isolated by a two-step collagenase perfusion technique with modifications. Briefly, the inferior vena cava (IVC) was cannulated with a 24-gauge 3/4 inch angiocatheter (BD) and the portal vein was cut. The liver was perfused via the inferior vena cava with 100 mL of Liver Perfusion Medium (LP, Invitrogen) at 37 °C, followed by perfusion with 100 mL of collagenase type IV (Wellington) in HBSS containing Ca^{2+} and Mg^{2+} (GIBCO). After the liver was digested, it was dissected out and cut into small pieces and passed through a 100 μm strainer (Falcon). Hepatocytes were separated from non-parenchymal cells (NPCs) by low-speed centrifugation (50 g × 5 mins × 3, brake = 2), and further purified by Percoll gradient centrifugation (50 % v/v, Sigma). For 3D culture, hepatocytes were embedded in growth-factor reduced (GFR) matrigel (BD), at approximately 1000 cells per 20 μL of matrigel droplets. William E media containing 1% (v/v) Glutamax, 1% (v/v) Non-Essential Amino Acids, 1% (v/v) penicillin/streptomycin (all from Gibco), 0.2% (v/v) normocin (Invivogen), 2% (v/v) B27 (Gibco), 1% (v/v) N2 supplement (Gibco), 100 mM nicotinamide (Sigma-Aldrich), 1.25 mM N-acetylcysteine (Sigma-Aldrich), 10 μM Y27632 (Peprotech), 1 μM A83-01 (Tocris) was used as basal media. Expansion media contained 3 μM CHIR99021 (Peprotech), 25 ng/mL EGF (Peprotech), 50 ng/mL HGF (Peprotech) and 100 ng/mL TNFα (Peprotech). Media was replaced every 2 – 3 days. After approximately 2 weeks in culture, matrigel was digested with dispase (Stem Cell Technologies), and released intact organoids were embedded in new matrigel droplets and cultured for another one to two weeks. Of note, hepatocyte organoids were not dissociated by dispase. From the second passage onwards, after dispase digestion of matrigel, released organoids were further incubated with TrypLE Express (Gibco) for 5 minutes at 37 °C. Then, 3D colonies were broken up into multiple-cell aggregates by gentle pipetting. To ensure high viability of hepatocytes, prolonged enzyme incubation or mechanical dissociation that resulted in single-cell suspension was avoided. Dissociated cell aggregates were embedded in matrigel at appropriate densities (usually at 500 – 2000 cells per 20 μL drops). Remaining cells were frozen in Bambanker (Wako) at −80 °C and could be thawed following standard procedures for subsequent cultures. For long term culture, media was supplemented with 50 ng/mL noggin (Peprotech) for the first 4 – 7 days of culture from the second passage onwards. Cultures were typically passaged every 14 – 20 days, when the size of organoids was > 200 – 300 μm, or when the matrigel droplets were overcrowded. For culture without TNFα, the cytokine was omitted from the media, but otherwise contained all other factors present in the standard expansion media. For culture with IL-6, 50 ng/ml IL-6 was used in the expansion media without TNFα. For hepatocyte differentiation, hepatocytes were cultured in expansion media for approximately 2 weeks, and then switched to differentiation media for the last 3 – 5 days of culture. EGF- induction media contained 25 ng/ml EGF, 50 ng/ml HGF and 3 μM

dexamethasone (Tocris), and Wnt- induction media contained 3 μM CHIR 99021 and 3 μM dexamethasone, in the basal media described above.

High content imaging

The Cellnsight CX7 High-Content Screening (HCS) Platform (Thermo Fisher Scientific) was used for colony counting and nuclear intensity measurements. Briefly, cultures were incubated with media containing 1 μg/mL Hoechst 33342, 2 μg/mL propidium iodide (both from Life Technologies), 5 μM reserpine (Sigma-Aldrich), 1:250 HCS LipidTOX (Invitrogen) for 30 – 60 minutes in the presence of 50 % (v/v) dispase. 3D organoids were released from matrigel by gentle pipetting, washed twice with media and then transferred to a 96-well plate (Corning) for imaging. The colonies were imaged on wide-field, confocal Z-stack, and bright-field and were quantified using HCS Studio Cell Analysis Software (Thermo Fisher). Cell debris or dead cells were excluded based on colony size, nuclear intensity and length-to-width ratio, and the same threshold was applied for the colony counting of hepatocytes cultured with or without TNFα.

Real time quantitative PCR

3D cultures were harvested from matrigel using dispase and total RNA was purified using the RNeasy mini kit (Qiagen) according to the manufacturer's instructions. The total RNA was reverse-transcribed using random primers (High Capacity cDNA Reverse Transcription kit, Life Technologies). Gene expression was assayed by real-time PCR using TaqMan Gene Expression Assays (Applied Biosystems) on an ABI 7900HT real-time PCR system. GAPDH was used as an internal control for amount of RNA input in each well. RT-PCR probes used are shown in Table 1. Measurements were performed in triplicate for each biological sample.

Antibody staining of organoids

For whole-mount organoid staining, organoids were fixed in 2% paraformaldehyde at 4 °C overnight, washed twice in PBS and then placed in PBS-Tw (PBS, 10% v/v NDS, 0.1% v/v Tween) for 30 minutes in glass staining dishes. Primary antibody was applied to organoids in PBS-Tw. Alternatively, for nuclear antibodies PBS-Tx (PBS, 0.01% v/v TritonX-100 was used to dilute the antibodies at the concentrations listed in Table 2. Organoids were incubated overnight at 4 °C and then were washed 3x in PBSTw. Secondary antibodies were applied in PBS-Tw for 1 hour followed by 3 washes in PBS-Tw. DAPI was added at a concentration of 300 μM to stain nuclei before visualization. Organoids were imaged on a Zeiss Cell Observer SD spinning disk microscope. Images were processed using Photoshop.

For staining of organoid sections,_organoids were fixed in 2% paraformaldehyde overnight, washed in PBS 2x and then placed in a 50 μl drop of Histogel (Thermo Scientific). The hardened organoid/Histogel droplet was placed in 2 % methylene blue for 5 minutes to stain and follow the organoids during subsequent processing steps. The organoid/Histogel drops were washed 3x in PBS to remove the excess methylene blue, and then placed in 30 % sucrose for 2 hours followed by a 1 hour incubation in a 1:1 mixture of 30 % sucrose/OCT. The droplet was transferred to 100 % OCT for 15 minutes and then moved into new OCT to freeze the organoids in blocks. 7 μm sections were cut on a cryostat (Leica CM3050S) at

−30 °C. The presence of organoids in the section could be verified by the presence of methylene blue stained cells on the slides. Slides were stored at −20 °C. When ready to stain with antibody, slides were air dried at room temperature for 30 minutes. A hydrophobic barrier was drawn around each section with an ImmedgePen (Vector Labs) and then samples were fixed for 5 minutes in 4 % PFA followed by 2 rinses in PBS. Tris-based antigen retrieval was performed on the slides followed by blocking in 10 % NDS-PBS-Tw. Primary antibodies were diluted in PBS-Tw and applied to the sections at the appropriate dilution as listed in Table 2. Incubations were performed at 4 °C overnight followed by 2 washes in PBS-Tw. Secondary antibody incubation was performed in PBS-Tw at room temperature for 1 hour. Slides were mounted with ProlongGold with Dapi (Invitrogen) before visualization. Imaging was performed on a Zeiss Imager Z.2 or a Zeiss Cell Observer SD spinning disk microscope. Image processing was performed using Photoshop.

Functional assays.

Albumin secretion assay is performed using the mouse albumin ELISA kit (Assaypro) according to manufacturer's instructions. Briefly, hepatocytes in expansion media (3, 5, and 7 months) were switched to EGF- or CHIR- induction media during the last 4 – 6 days of culture. Culture media were harvested for measurements two days after the last media change. Freshly isolated adult primary hepatocytes from two mice (50 K cells) were plated on 2D collagen-coated plate in EGF induction media and media was harvested 4 days later for measurements. CYP3A11 activity was measured using the P450-Glo™ CYP3A4 assay system according to manufacturer's instructions. Hepatocytes in expansion media were switched to switched to EGF- or Wnt- induction media for the last 4 – 6 days of culture. 3D hepatocytes, and control cells HepG2 and HEK293T (both in 2D culture) were incubated with 3 μM of luciferin-IPA in 200 μL of RPMI (10 % v/v FBS) overnight for the measurement of CYP3A11 activity. To evaluate LDL uptake, hepatocytes in expansion media were incubated overnight with LDL conjugated with DyLight™-550 (LDL Uptake Assay Kit, Abcam ab1331267). For visualization of LDL uptake, 3D hepatocytes in matrigel were treated with dispase to release intact organoids and excess dyes were removed with triple washes. To assess secretion into bile canaliculi, hepatocytes in EGF- induction media were incubated with fluorescein diacetate (Santa Cruz Biotechnology sc-294598) for 15 – 30 min at 37 °C, and fluorescent dye was replaced with culture media and visualized immediately. To evaluate glycogen storage, 3D hepatocytes in expansion media were embedded in paraffin section and stained with Periodic Acid-Schiff kit (Sigma Aldrich, 395B-1KT) according to manufacturer's instructions. Negative control slides were treated with human saliva containing α-amylase.

Lentiviral gene delivery

At 24 hours prior to transfection, HEK293T cells were plated in 6-well plate at 8×10^5 cells per well in DMEM (10 % v/v FBS). Cells growing at ~70-80 % confluency were transfected with 1 μg of pLKO.1-puro-CMV-TurboGFP (Sigma Aldrich) along with 2nd generation lentiviral packaging and envelope plasmids, 0.75 μg of psPAX2 and 0.25 μg of pMD.2g (gifts from D. Trono, Addgene #12260, #12259). At 36 hours post transfection, the media containing lentiviral particles was collected and passed through a 0.45 μm filter. Polybrene was added to a final concentration of 4 μg/mL. 3D hepatocyte colonies released from

matrigel were resuspended in expansion or EGF-induction media in ultra-low attachment plate for lentiviral infection. The filtered media containing lentivirus was added at a 1:1 (v/v) dilution to target hepatocyte organoids. A second infection was performed at 60 hours post transfection. GFP expression was visualized at 48 hours after the first infection. For 2D visualization of hepatocytes, hepatocytes were transitioned to geltrex-coated 2D culture in expansion media (2 % v/v FBS) at day 5 post second infection, and imaged 2 days later on a Leica DMI 600B microscope.

Hepatocyte and HUVEC co-culture

GFP expressing human umbilical vein endothelial cells (GFP-HUVECs) were cultured according to manufacturer's instructions (Angioproteomie). Briefly, GFP-HUVECs were expanded on a Geltrex-coated (Life Technologies) 6-well plate in EGM-2 Bullet kit media (Lonza) and trypsinized prior to co-culture experiments. For co-culture experiments, 3D hepatocyte organoids (in the order of hundreds) were resuspended with GFP-HUVECs on a 96-well (10,000 – 20,000 cells) or 24-well (60,000 cells) flat bottom ultra-low attachment plate (Corning) in 1:1 (v/v) dilution of hepatocyte expansion media and HUVEC media and were cultured for approximately 2 weeks.

Single-cell RNA sequencing

Single-cell RNA sequencing was performed using the 10x Genomics Chromium System (Zheng et al., 2017). Hepatocytes were derived from one male and one female mouse, cultured for a total of 75 and 97 days, respectively. Briefly, after passaging, hepatocytes were cultured in expansion media for 12 days (termed '*expansion*': 3 μM CHIR 99021, 25 ng/mL EGF, 50 ng/mL HGF and 100 ng/mL TNFα) or switched to EGF- induction media (termed '*induction*': 25 ng/mL EGF, 50 ng/mL HGF and 3 μM dexamethasone) for the last 4 days of culture (i.e., day 9 – 12). To obtain single-cell suspension, the cultures were incubated with dispase for 20 minutes, washed twice with William E media and further incubated with 0.25 % Trypsin-EDTA solution (Gibco) for 30 minutes. The organoids were then gently dissociated by mechanical pipetting, washed twice with William E media to remove cell debris and then flow through a 40 μm strainer to remove cell aggregates. Cell counts were performed using the Cellometer K2 (Nexelcom). We pooled together the cells from one male and one female and loaded a total of ~1,200 cells from each culture condition on the Chromium Instrument (10x Genomics, Pleasanton, CA, USA).

Single-cell RNA-seq library was generated using GemCode Single-Cell 3′ Gel Bead and Library V2 Kit. Single cell library was loaded on Illumina HiSeq 4000 Systems with 2 × 100 pair-end kits with the following reads: 26 bases Read 1 (cell barcode and UMI), 8 bases i7 Index 1 (sample index) and 98 bases Read 2 (transcript). The Cell Ranger Software (Version 2.1.1) was used to perform sample de-multiplexing, barcode processing and 3' UMI counting. For 'expansion' culture, approximately 1208 cells were sequenced, with the mean reads of 243, 654 per cell and median genes of 3832 per cell, median UMI counts of 22,969 per cells. For 'induction' culture, approximately 1275 cells were sequenced, with the mean reads of 43, 292 per cell and median genes of 1986 per cell, median UMI counts of 22,969 per cells. Dataset for 3-month old primary hepatocytes (termed 'primary'), derived from two female and one male mice, were obtained from GEO database with the accession numbers

GSM3040892, GSM3040898 and GSM3040899, and was previously described here (The Tabula Muris Consortium et al., 2017). Data obtained from GEO database was reprocessed using Cell Ranger version 2.1.1 with mm10 as the reference genome. Single cell data was analyzed using standard workflow on Seurat R Package (Butler et al., 2018). Female-derived cells could be distinguished from male-derived cells based on the *Xist* gene expression. Cells that have at least one UMI for *Xist* gene are assigned as female cells, while the remaining are assigned as male cells. For the analysis of the 'expansion' dataset, gene-barcode matrix was filtered based on number of genes detected per cell (< 200 genes/cell excluded) and percent.mito (> 25 % excluded), and genes that are expressed in fewer than 10 cells were excluded. For the joint-analysis 'expansion', 'induction' and primary hepatocytes, cells with < 500 or > 6000 genes/cells and > 25 % percent.mito were excluded. After filtering, we obtained 1192 cells from exp (592 male, 600 female) and 1245 cell from induction media (811 male cells, 434 female cells). These cells were analyzed by PCA, and the top 10 PCs were selected, based on elbow plot for downstream clustering analysis. t-SNE plot was used to visualize the clusters. The average gene expression (UMI count) of a cluster, and differentially expressed gene between clusters were also determined using Seurat R Package. Gene ontology analysis was performed using the Gene Ontology Consortium web platform described previously (Ashburner et al., 2000).

Immunohistochemistry and Immunocytochemistry of engraftment in Fah- tissues

Liver samples were isolated from FAH- hosts, fixed in 10% neutral buffered formalin pH7.4 overnight and processed for embedding in paraffin. 5 μm sections were cut, de-paraffinized and re-hydrated by standard methods and processed for further staining. Immunohistochemistry to detect FAH in liver samples was performed as previously described (Wang et al., 2002). For immunofluorescence staining, Citrate or Tris-based antigen retrieval (Vector Labs) was performed on de-parafinized sections. Slides to be stained with anti-TBX3 antibody were treated with Biotin/Avidin Blocking reagent (Vector labs). All slides were blocked and then incubated in primary antibodies for 1 hour at room temperature or overnight at 4°C (Table 2). Samples stained for TBX3 were incubated with biotinylated secondary antibody followed by incubation with Streptavidin-647. Other slides were incubated in secondary antibodies against the respective primary antibody host for 1 hour at room temperature. Slides were washed and mounted using ProlongGold with Dapi (Invitrogen) for visualization. Samples were imaged using a Zeiss Imager Z.2, Zeiss Cell Observer SD spinning disk microscope or a Cellnsight CX7 High-Content Screening (HCS) Platform (Thermo Fisher Scientific).

In Situ Hybridization

Paraffin-embedded tissue sections were cut at 5 μm thickness and processed for detection of mRNA using the manual RNAscope 2.5 HD Assay-Red or RNAscope 2.5 HD Duplex Kits (Advanced Cell Diagnostics, Hayward CA) according to the manufacturer's instructions. Images were taken at 10x and 20x magnification on a Zeiss Imager Z.2. Images were processed using Photoshop. Probes used in this study were Fah (target region: 490-1364), Wnt9b (target region: 706-1637), Wnt2 (target region: 857-2086), Rspo3 (target region: 731-2164), Rspo 1 (target region: 550-1679), Rspo2 (target region: 537-1452), Rspo4 (target

region: 1180-2202), CD31/Pecam (target region: 915-1827), CD45/Ptprc (target region: 2922-3866), TNFα (target region: 41-1587).

Transplantation

Fah$^{-/-}$ mice (*FAH* $^{\Delta exon5}$) (Overturf et al., 1996) were maintained on a C57BL/6J background and treated with 2-(2-nitro-4-trifluoromethylbenzoyl)-1,3-cyclohexanedione in drinking water. Animal transplantation was conducted in accordance with protocol IS00445 of the Institutional Review Committee at Oregon Health and Science University. Hepatocytes were derived from 8-week old mice of wild type or *Axin2-rtTA;Tet-O-H2B:GFP* background (Wang et al., 2015). In the first experiment, hepatocytes derived from three mice were cultured in expansion media for 17-, 17- and 21- days, respectively. In the second experiment, hepatocytes derived from three mice were expanded for 48-, 55- and 105- days, respectively. For transplantation, intact organoids were released from matrigel by dispase treatment. 3D organoids were resuspended in expansion media supplemented with 2 % FBS (Omega Scientific) and transported overnight on ice for transplantation. Transplantation was performed according to previously described protocol (Azuma et al., 2007; Li et al., 2017). One day before transplantation, Fah$^{-/-}$ mice were taken off NTBC. 3D organoids were injected intra-splenically the following day. In the first experiment, mice were put on five NTBC ON cycles (first cycle: 8 d off, 3 d on; second cycle: 7 d off, 5 d on; third cycle: 16 d off, 5 d on; fourth cycle: 7 d off, 4 d on; fifth cycle: 21 d off, 3 d on; final 25 d off). In the second experiment, mice were put on three NTBC cycles (first cycle: 14 d off, 7 d on; second cycle: 14 d off, 4 d on; third cycle: 21 d off, 3 d on; final 21 d off) or four cycles (first cycle: 8 d off, 4 d on; second cycle: 14 d off, 4 d on; third cycle: 21 d off, 3 d on; fourth cycle: 24 d off, 4 d on; final 33 d or 44 d off). The livers of transplanted mice were harvested at various time points after transplantation and evaluated by FAH antibody staining. FAH engraftment area was determined using ImageJ.

Supplementary Material

Refer to Web version on PubMed Central for supplementary material.

ACKNOWLEDGEMENTS

We are grateful to A. Haft, L. Wakefield and M. Finegold for assistance with transplantation experiments; K. Karlson for technical assistance with single-cell RNA-seq analysis; K.M. Loh, L.T. Ang, A.J. Sarkar and E.J. Rulifson for critically reading the manuscript; and the Stanford Functional Genomics Facility for 10x Genomics single-cell library preparation and Genome Sequencing Service Center for 10x Genomics library sequencing. This study was supported by the Howard Hughes Medical Institute (HHMI) and the California Institute for Regenerative Medicine(CIRM); the Genome Sequencing Service Center of the Stanford Center for Genomics and Personalized Medicine Sequencing Center was supported by NIH grant S10OD020141. P.W. is an Ernest and Amelia Gallo Endowed Postdoctoral Fellow supported by the Stanford Child Research Institute.

REFERENCES

Akerman P, Cote P, Yang SQ, McClain C, Nelson S, Bagby GJ, and Diehl AM (1992). Antibodies to tumor necrosis factor-alpha inhibit liver regeneration after partial hepatectomy. Am. J. Physiol 263, G579–G585. [PubMed: 1415718]

Arnett HA, Mason J, Marino M, Suzuki K, Matsushima GK, and Ting JP (2001). TNF alpha promotes proliferation of oligodendrocyte progenitors and remyelination. Nat. Neurosci 4, 1116–1122. [PubMed: 11600888]

Ashburner M, Ball CA, Blake JA, Botstein D, Butler H, Cherry JM, Davis AP, Dolinski K, Dwight SS, Eppig JT, et al. (2000). Gene ontology: tool for the unification of biology. The Gene Ontology Consortium. Nature Genetics 25, 25–29. [PubMed: 10802651]

Aurora AB, and Olson EN (2014). Immune modulation of stem cells and regeneration. Cell Stem Cell 15, 14–25. [PubMed: 24996166]

Azuma H, Paulk N, Ranade A, Dorrell C, Al-Dhalimy M, Ellis E, Strom S, Kay MA, Finegold M, and Grompe M (2007). Robust expansion of human hepatocytes in Fah−/−/Rag2−/−/Il2rg−/− mice. Nat Biotechnol 25, 903–910. [PubMed: 17664939]

Beg AA, Sha WC, Bronson RT, Ghosh S, and Baltimore D (1995). Embryonic lethality and liver degeneration in mice lacking the RelA component of NF-kappa B. Nature 376, 167–170. [PubMed: 7603567]

Benhamouche S, Decaens T, Godard C, Chambrey R, Rickman DS, Moinard C, Vasseur-Cognet M, Kuo CJ, Kahn A, Perret C, et al. (2006). Apc tumor suppressor gene is the “zonation-keeper” of mouse liver. Devcel 10, 759–770.

Borkham-Kamphorst E, van de Leur E, Zimmermann HW, Karlmark KR, Tihaa L, Haas U, Tacke F, Berger T, Mak TW, and Weiskirchen R (2013). Protective effects of lipocalin-2 (LCN2) in acute liver injury suggest a novel function in liver homeostasis. Biochim. Biophys. Acta 1832, 660–673. [PubMed: 23376114]

Broutier L, Andersson-Rolf A, Hindley CJ, Boj SF, Clevers H, Koo B-K, and Huch M (2016). Culture and establishment of self-renewing human and mouse adult liver and pancreas 3D organoids and their genetic manipulation. Nat Protoc 11, 1724–1743. [PubMed: 27560176]

Broutier L, Mastrogiovanni G, Verstegen MM, Francies HE, Gavarró LM, Bradshaw CR, Allen GE, Arnes-Benito R, Sidorova O, Gaspersz MP, et al. (2017). Human primary liver cancer–derived organoid cultures for disease modeling and drug screening. Nature Publishing Group 23, 1–19.

Butler A, Hoffman P, Smibert P, Papalexi E, and Satija R (2018). Integrating single-cell transcriptomic data across different conditions, technologies, and species. Nat Biotechnol 36, 411–420. [PubMed: 29608179]

Camp JG, Sekine K, Gerber T, Loeffler-Wirth H, Binder H, Gac M, Kanton S, Kageyama J, Damm G, Seehofer D, et al. (2017). Multilineage communication regulates human liver bud development from pluripotency. Nature Publishing Group 109, 1–22.

Chen C-C, Wang L, Plikus MV, Jiang TX, Murray PJ, Ramos R, Guerrero-Juarez CF, Hughes MW, Lee OK, Shi S, et al. (2015). Organ-level quorum sensing directs regeneration in hair stem cell populations. Cell 161, 277–290. [PubMed: 25860610]

Clevers H, Loh KM, and Nusse R (2014). Stem cell signaling. An integral program for tissue renewal and regeneration: Wnt signaling and stem cell control. Science 346, 1248012–1248012. [PubMed: 25278615]

Costa RH, Kalinichenko VV, Holterman A-XL, and Wang X (2003). Transcription factors in liver development, differentiation, and regeneration. Hepatology 38, 1331–1347. [PubMed: 14647040]

Cressman DE, Greenbaum LE, DeAngelis RA, Ciliberto G, Furth EE, Poli V, and Taub R (1996). Liver failure and defective hepatocyte regeneration in interleukin-6-deficient mice. Science 274, 1379–1383. [PubMed: 8910279]

de Lau W, Peng WC, Gros P, and Clevers H (2014). The R-spondin/Lgr5/Rnf43 module: regulator of Wnt signal strength. Genes & Development 28, 305–316. [PubMed: 24532711]

Edmondson R, Broglie JJ, Adcock AF, and Yang L (2014). Three-dimensional cell culture systems and their applications in drug discovery and cell-based biosensors. Assay Drug Dev Technol 12, 207–218. [PubMed: 24831787]

Gerstenfeld LC, Cho TJ, Kon T, Aizawa T, Tsay A, Fitch J, Barnes GL, Graves DT, and Einhorn TA (2003). Impaired Fracture Healing in the Absence of TNF-α Signaling: The Role of TNF-α in Endochondral Cartilage Resorption. Journal of Bone and Mineral Research 18, 1584–1592. [PubMed: 12968667]

Grompe M, Al-Dhalimy M, Finegold M, Ou CN, Burlingame T, Kennaway NG, and Soriano P (1993). Loss of fumarylacetoacetate hydrolase is responsible for the neonatal hepatic dysfunction phenotype of lethal albino mice. Genes & Development 7, 2298–2307. [PubMed: 8253378]

Hailfinger S, Jaworski M, Braeuning A, Buchmann A, and Schwarz M (2006). Zonal gene expression in murine liver: Lessons from tumors. Hepatology 43, 407–414. [PubMed: 16496347]

Halpern KB, Shenhav R, Matcovitch-Natan O, Tóth B, Lemze D, Golan M, Massasa EE, Baydatch S, Landen S, Moor AE, et al. (2017). Single-cell spatial reconstruction reveals global division of labour in the mammalian liver. Nature 542, 352–356. [PubMed: 28166538]

Hu Y, Xue J, Yang Y, Zhou X, Qin C, Zheng M, Zhu H, Liu Y, Liu W, Lou G, et al. (2015). Lipocalin 2 Upregulation Protects Hepatocytes from IL1-β-Induced Stress. Cell. Physiol. Biochem. 36, 753–762. [PubMed: 26021263]

Huch M, and Koo B-K (2015). Modeling mouse and human development using organoid cultures. Development 142, 3113–3125. [PubMed: 26395140]

Huch M, Dorrell C, Boj SF, van Es JH, Li VSW, van de Wetering M, Sato T, Hamer K, Sasaki N, Finegold MJ, et al. (2013). In vitro expansion of single Lgr5+ liver stem cells induced by Wnt-driven regeneration. Nature 494, 247–250. [PubMed: 23354049]

Huch M, Gehart H, van Boxtel R, Hamer K, Blokzijl F, Verstegen MMA, Ellis E, van Wenum M, Fuchs SA, de Ligt J, et al. (2015). Long-Term Culture of Genome-Stable Bipotent Stem Cells from Adult Human Liver. Cell 160, 299–312. [PubMed: 25533785]

Jeffery V, Goldson AJ, Dainty JR, Chieppa M, and Sobolewski A (2017). IL-6 Signaling Regulates Small Intestinal Crypt Homeostasis. J. Immunol. 199, 304–311. [PubMed: 28550196]

Kang L-I, Mars W, and Michalopoulos G (2012). Signals and Cells Involved in Regulating Liver Regeneration. Cells 1, 1261–1292. [PubMed: 24710554]

Karin M, and Clevers H (2016). Reparative inflammation takes charge of tissue regeneration. Nature 529, 307–315. [PubMed: 26791721]

Karin M, and Greten FR (2005). NF-kappaB: linking inflammation and immunity to cancer development and progression. Nat. Rev. Immunol. 5, 749–759. [PubMed: 16175180]

Katsuda T, Kawamata M, Hagiwara K, Takahashi R-U, Yamamoto Y, Camargo FD, and Ochiya T (2016). Conversion of Terminally Committed Hepatocytes to Culturable Bipotent Progenitor Cells with Regenerative Capacity. Stem Cell 20, 1–16.

Kietzmann T (2017). Metabolic zonation of the liver_ The oxygen gradient revisited. Redox Biology 11, 622–630. [PubMed: 28126520]

Kirillova I, Chaisson M, and Fausto N (1999). Tumor necrosis factor induces DNA replication in hepatic cells through nuclear factor kappaB activation. Cell Growth Differ. 10, 819–828. [PubMed: 10616907]

Lee J, Homma T, Kurahashi T, Kang ES, and Fujii J (2015). Oxidative stress triggers lipid droplet accumulation in primary cultured hepatocytes by activating fatty acid synthesis. Biochem. Biophys. Res. Commun. 464, 229–235. [PubMed: 26116535]

Li B, Dorrell C, Canaday PS, Pelz C, Haft A, Finegold M, and Grompe M (2017). Adult Mouse Liver Contains Two Distinct Populations of Cholangiocytes. Stem Cell Reports 9, 478–489. [PubMed: 28689996]

Lin S, Nascimento EM, Gajera CR, Chen L, Neuhöfer P, Garbuzov A, Wang S, and Artandi SE (2018). Distributed hepatocytes expressing telomerase repopulate the liver in homeostasis and injury. Nature Publishing Group 556, 244–248.

Lindemans CA, Calafiore M, Mertelsmann AM, O'Connor MH, Dudakov JA, Jenq RR, Velardi E, Young LF, Smith OM, Lawrence G, et al. (2015). Interleukin-22 promotes intestinal-stem-cell-mediated epithelial regeneration. Nature 528, 560–564. [PubMed: 26649819]

Lindroos PM, Zarnegar R, and Michalopoulos GK (1991). Hepatocyte growth factor (hepatopoietin A) rapidly increases in plasma before DNA synthesis and liver regeneration stimulated by partial hepatectomy and carbon tetrachloride administration. Hepatology 13, 743–750. [PubMed: 1826282]

Magami Y, Azuma T, Inokuchi H, Kokuno S, Moriyasu F, Kawai K, and Hattori T (2002). Cell proliferation and renewal of normal hepatocytes and bile duct cells in adult mouse liver. Liver 22, 419–425. [PubMed: 12390477]

Michalopoulos GK, and DeFrances MC (1997). Liver regeneration. Science 276, 60–66. [PubMed: 9082986]

Michalopoulos GK (2007). Liver regeneration. J. Cell. Physiol. 213, 286–300. [PubMed: 17559071]

Michalopoulos GK (2017). Hepatostat: Liver regeneration and normal liver tissue maintenance. Hepatology 65, 1384–1392. [PubMed: 27997988]

Michalopoulos GK, Bowen WC, Mulè K, and Luo J (2003). HGF-, EGF-, and dexamethasone-induced gene expression patterns during formation of tissue in hepatic organoid cultures. Gene Expr. 11, 55–75. [PubMed: 12837037]

Miyajima A, Tanaka M, and Itoh T (2014). Stem/progenitor cells in liver development, homeostasis, regeneration, and reprogramming. Cell Stem Cell 14, 561–574. [PubMed: 24792114]

Muzumdar MD, Tasic B, Miyamichi K, Li L, and Luo L (2007). A global double-fluorescent Cre reporter mouse. Genesis 45, 593–605. [PubMed: 17868096]

Nusse YM, Savage AK, Marangoni P, Rosendahl-Huber AKM, Landman TA, de Sauvage FJ, Locksley RM, and Klein OD (2018). Parasitic helminths induce fetal-like reversion in the intestinal stem cell niche. Nature Publishing Group 559, 109–113.

Oguma K, Oshima H, Aoki M, Uchio R, Naka K, Nakamura S, Hirao A, Saya H, Taketo MM, and Oshima M (2008). Activated macrophages promote Wnt signalling through tumour necrosis factor-alpha in gastric tumour cells. Embo J. 27, 1671–1681. [PubMed: 18511911]

Overturf K, Al-Dhalimy M, Tanguay R, Brantly M, Ou CN, Finegold M, and Grompe M (1996). Hepatocytes corrected by gene therapy are selected in vivo in a murine model of hereditary tyrosinaemia type I. Nature Genetics 12, 266–273. [PubMed: 8589717]

Pikarsky E, Porat RM, Stein I, Abramovitch R, Amit S, Kasem S, Gutkovich-Pyest E, Urieli-Shoval S, Galun E, and Ben-Neriah Y (2004). NF-κB functions as a tumour promoter in inflammation-associated cancer. Nature Publishing Group 431, 461–466.

Planas-Paz L, Orsini V, Boulter L, Calabrese D, Pikiolek M, Nigsch F, Xie Y, Roma G, Donovan A, Marti P, et al. (2016). The RSPO-LGR4/5-ZNRF3/RNF43 module controls liver zonation and size. Nature Cell Biology 18, 467–479. [PubMed: 27088858]

Preziosi M, Okabe H, Poddar M, Singh S, and Monga SP (2018). Endothelial Wnts regulate β-catenin signaling in murine liver zonation and regeneration: A sequel to the Wnt-Wnt situation. Hepatol Commun 2, 845–860. [PubMed: 30027142]

Robinson MW, Harmon C, and O'Farrelly C (2016). Liver immunology and its role in inflammation and homeostasis. Cell. Mol. Immunol. 13, 267–276. [PubMed: 27063467]

Rocha AS, Vidal V, Mertz M, Kendall TJ, Charlet A, Okamoto H, and Schedl A (2015). The Angiocrine Factor Rspondin3 Is a Key Determinant of Liver Zonation. CellReports 13, 1757–1764.

Schwitalla S, Fingerle AA, Cammareri P, Nebelsiek T, Göktuna SI, Ziegler PK, Canli O, Heijmans J, Huels DJ, Moreaux G, et al. (2013). Intestinal Tumorigenesis Initiated by Dedifferentiation and Acquisition of Stem-Cell-like Properties. Cell 152, 25–38. [PubMed: 23273993]

Shimizu H, Miyazaki M, Wakabayashi Y, Mitsuhashi N, Kato A, Ito H, Nakagawa K, Yoshidome H, Kataoka M, and Nakajima N (2001a). Vascular endothelial growth factor secreted by replicating hepatocytes induces sinusoidal endothelial cell proliferation during regeneration after partial hepatectomy in rats. J. Hepatol. 34, 683–689. [PubMed: 11434614]

Shimizu H, Miyazaki M, Wakabayashi Y, Mitsuhashi N, Kato A, Ito H, Nakagawa K, Yoshidome H, Kataoka M, and Nakajima N (2001a). Vascular endothelial growth factor secreted by replicating hepatocytes induces sinusoidal endothelial cell proliferation during regeneration after partial hepatectomy in rats. J. Hepatol. 34, 683–689. [PubMed: 11434614]

Shimizu H, Mitsuhashi N, Ohtsuka M, Ito H, Kimura F, Ambiru S, Togawa A, Yoshidome H, Kato A, and Miyazaki M (2005). Vascular endothelial growth factor and angiopoietins regulate sinusoidal regeneration and remodeling after partial hepatectomy in rats. World J. Gastroenterol. 11, 7254–7260. [PubMed: 16437624]

Skov Olsen P, Boesby S, Kirkegaard P, Therkelsen K, Almdal T, Poulsen SS, and Nexø E (1988). Influence of epidermal growth factor on liver regeneration after partial hepatectomy in rats. Hepatology 8, 992–996. [PubMed: 3047041]

Su T, Bondar T, Zhou X, Zhang C, He H, and Medzhitov R (2015). Two-signal requirement for growth-promoting function of Yap in hepatocytes. eLife 4, 1060–23.

Takebe T, Sekine K, Enomura M, Koike H, Kimura M, Ogaeri T, Zhang R-R, Ueno Y, Zheng Y-W, Koike N, et al. (2013). Vascularized and functional human liver from an iPSC-derived organ bud transplant. Nature 499, 481–484. [PubMed: 23823721]

Takebe T, Zhang R-R, Koike H, Kimura M, Yoshizawa E, Enomura M, Koike N, Sekine K, and Taniguchi H (2014). Generation of a vascularized and functional human liver from an iPSC-derived organ bud transplant. Nat Protoc 9, 396–409. [PubMed: 24457331]

Taniguchi E, Sakisaka S, Matsuo K, Tanikawa K, and Sata M (2001). Expression and role of vascular endothelial growth factor in liver regeneration after partial hepatectomy in rats. J. Histochem. Cytochem. 49, 121–130 [PubMed: 11118484]

The Tabula Muris Consortium, Quake SR, Wyss-Coray T, and Darmanis S (2017). Single-cell transcriptomic characterization of 20 organs and tissues from individual mice creates a Tabula Muris.

Torbenson M, Yang SQ, Liu HZ, Huang J, Gage W, and Diehl AM (2002). STAT-3 overexpression and p21 up-regulation accompany impaired regeneration of fatty livers. The American Journal of Pathology 161, 155–161. [PubMed: 12107100]

van Amerongen R, Bowman AN, and Nusse R (2012). Developmental Stage and Time Dictate the Fate of Wnt/β-Catenin-Responsive Stem Cells in the Mammary Gland. Cell Stem Cell 11, 387–400. [PubMed: 22863533]

Wang B, Zhao L, Fish M, Logan CY, and Nusse R (2015). Self-renewing diploid Axin2(+) cells fuel homeostatic renewal of the liver. Nature Publishing Group 524, 180–185.

Warner JR (1999). The economics of ribosome biosynthesis in yeast. Trends Biochem. Sci. 24, 437–440. [PubMed: 10542411]

Webber EM, Bruix J, Pierce RH, and Fausto N (1998). Tumor necrosis factor primes hepatocytes for DNA replication in the rat. Hepatology 28, 1226–1234. [PubMed: 9794905]

Yamada Y, Kirillova I, Peschon JJ, and Fausto N (1997). Initiation of liver growth by tumor necrosis factor: deficient liver regeneration in mice lacking type I tumor necrosis factor receptor. Proc Natl Acad Sci USA 94, 1441–1446. [PubMed: 9037072]

Yimlamai D, Christodoulou C, Galli GG, Yanger K, Pepe-Mooney B, Gurung B, Shrestha K, Cahan P, Stanger Ben Z, and Camargo FD (2014). Hippo Pathway Activity Influences Liver Cell Fate. Cell 157, 1324–1338. [PubMed: 24906150]

Yu H-MI, Liu B, Costantini F, and Hsu W (2007). Impaired neural development caused by inducible expression of Axin in transgenic mice. Mech. Dev. 124, 146–156. [PubMed: 17123792]

Zheng GXY, Terry JM, Belgrader P, Ryvkin P, Bent ZW, Wilson R, Ziraldo SB, Wheeler TD, McDermott GP, Zhu J, et al. (2017). Massively parallel digital transcriptional profiling of single cells. Nature Communications 8, 1–12.

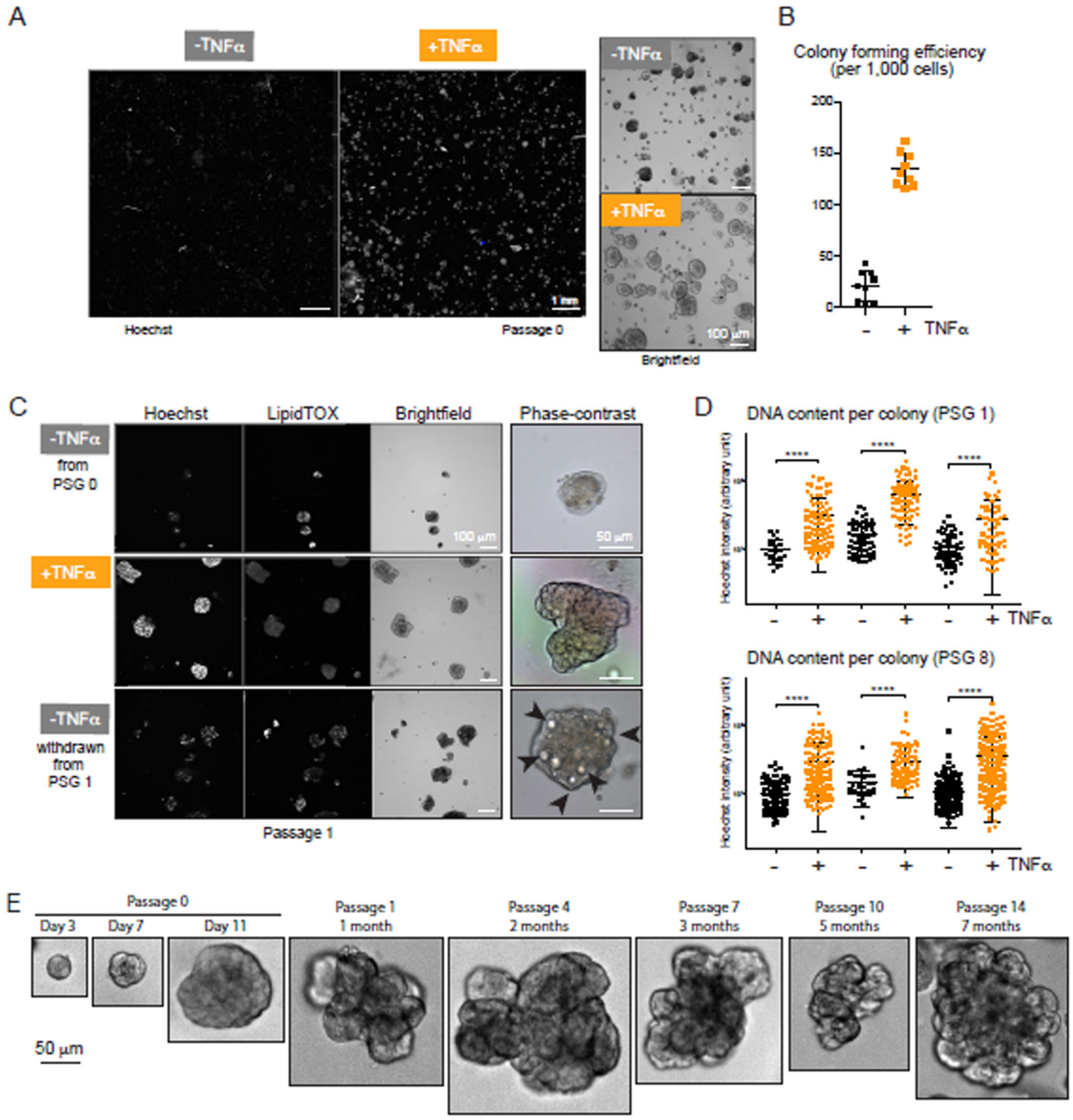

Figure 1. TNFα promotes the expansion of primary hepatocytes in 3D culture.

(A)Confocal (montage) and brightfield images of freshly isolated primary mouse hepatocytes cultured in expansion media, with or without TNFα for 2 weeks. Hoechst intensities are shown on the same scale.

(B) Colony forming efficiency of hepatocytes cultured with or without TNFα. Approximately 1,000 cells were seeded and colony count was performed after 2 weeks. Data are represented as mean ± SEM of three biological replicates.

(C) Images of hepatocyte cultures at passage 1. Cells cultured continuously without TNFα (top), with TNFα (middle), or with TNFα withdrawn after passaging (bottom). Phase-contrast images shown to highlight lipid droplets (arrowheads).

(D) Scatter plots showing Hoechst intensity per hepatocyte colony. Hepatocytes were cultured continuously with TNFα, or with TNFα withdrawn from culture media at passage 1 (top) or at passage 8 (bottom). Measurements were performed at least one week after TNFα withdrawal. Mann-Whitney U test, ****$p < 0.0001$. Data for each biological replicate are shown.

(E) Representative images of long-term cultured hepatocytes in the presence of TNFα.

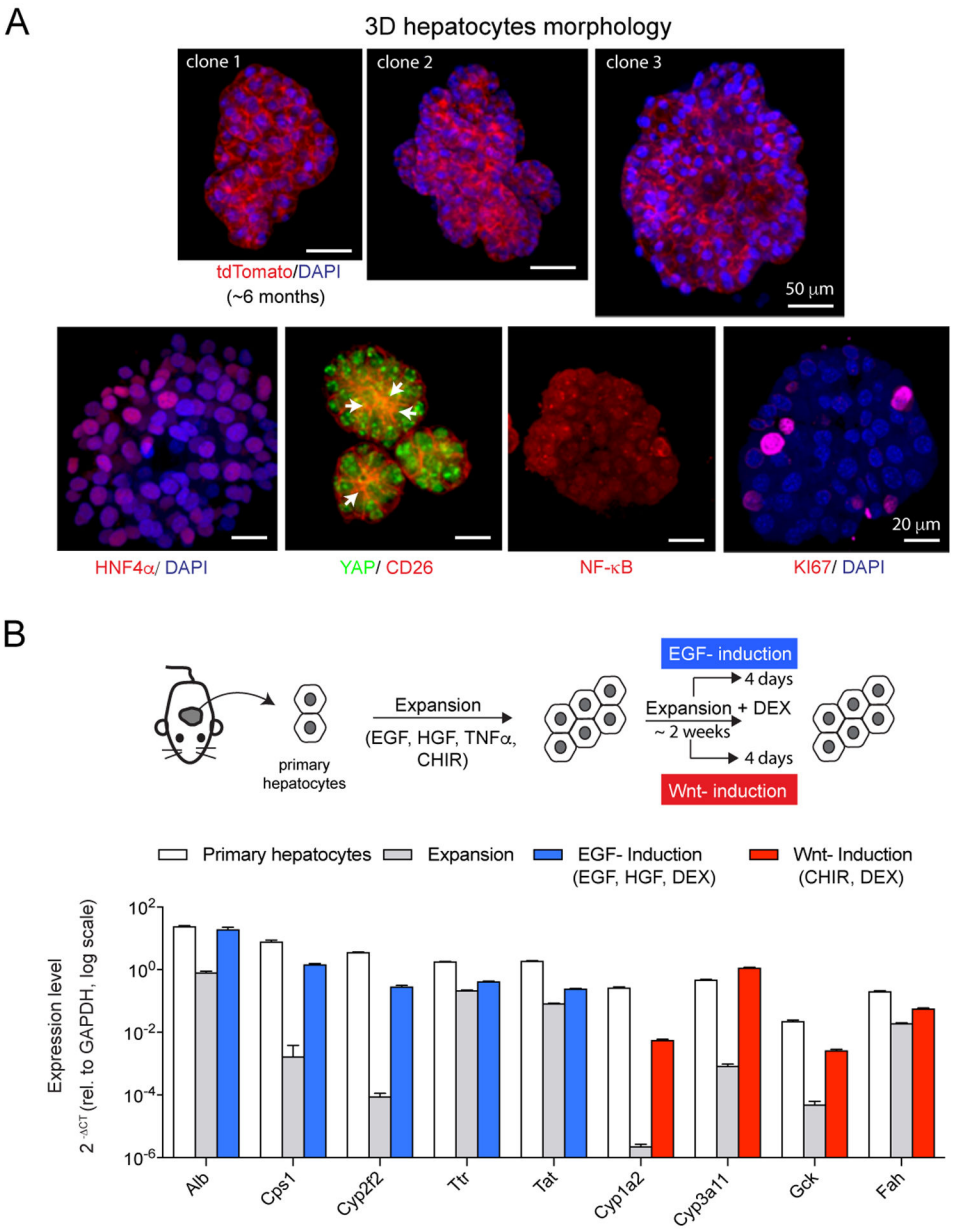

Figure 2. Expression and modulation of functional markers in 3D hepatocytes.

(A) Confocal images (Z-stack projection) of hepatocyte colonies constitutively expressing membrane tdTomato (top) or stained for various markers and visualized by immunofluorescence (bottom). Arrows mark CD26+ bile canaliculi. Scale bars = 50 μm (top), 20 μm (bottom).

(B) Gene expression analysis of primary hepatocytes and cultured hepatocytes evaluated by q-PCR. Data are represented as mean ± SEM of three independent measurements.

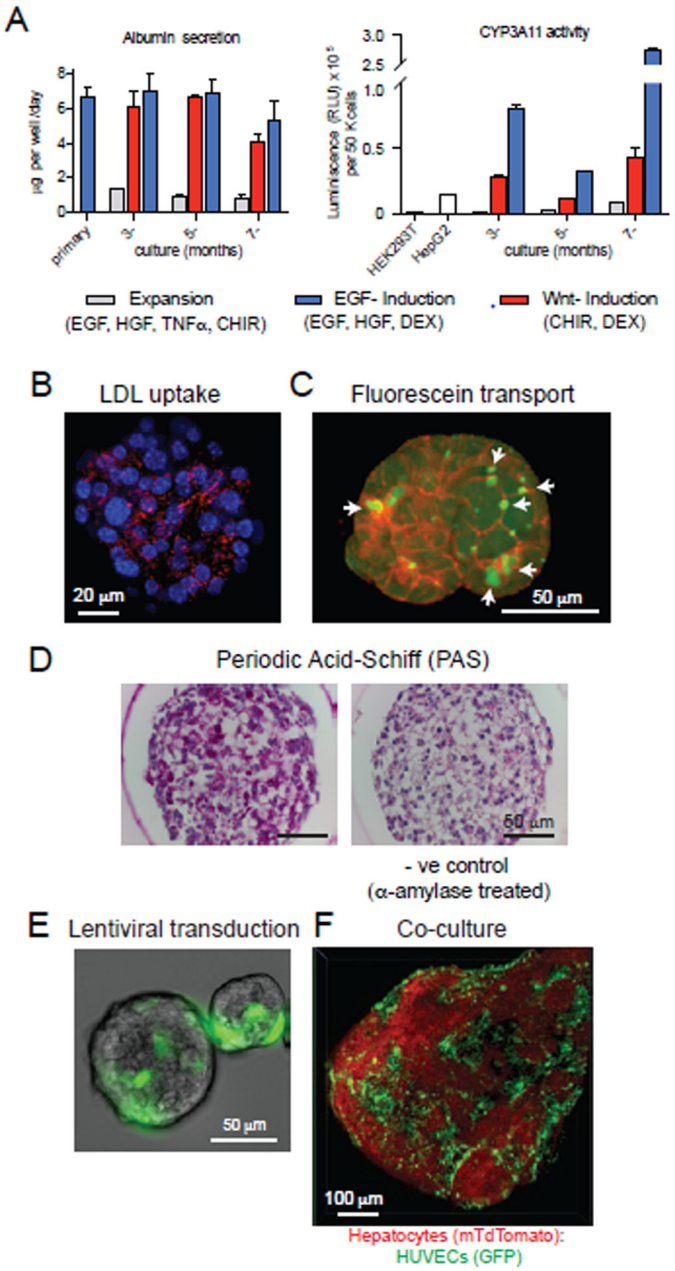

Figure 3. 3D hepatocytes display functional activities.

(A)Albumin secretion measured by mouse albumin ELISA assay (left) and CYP3A11 activity measured by P450-Glo™ CYP3A assay using luciferin-IPA as a substrate (right).

(B)LDL uptake visualized by LDL conjugated with DyLight™-550.

(C) Fluorescein diacetate uptake and secretion into bile canaliculi structures (arrowheads).

(D) Glycogen storage visualized by PAS staining.

(E) Overlay of wide-field fluorescence and BF images of 3D hepatocytes expressing GFP introduced by lentiviral transduction.

(F) Confocal Z stack-projection of 3D hepatocytes expressing mTdTomato and GFP-HUVECs aggregate, two weeks after the initiation of co-culture.

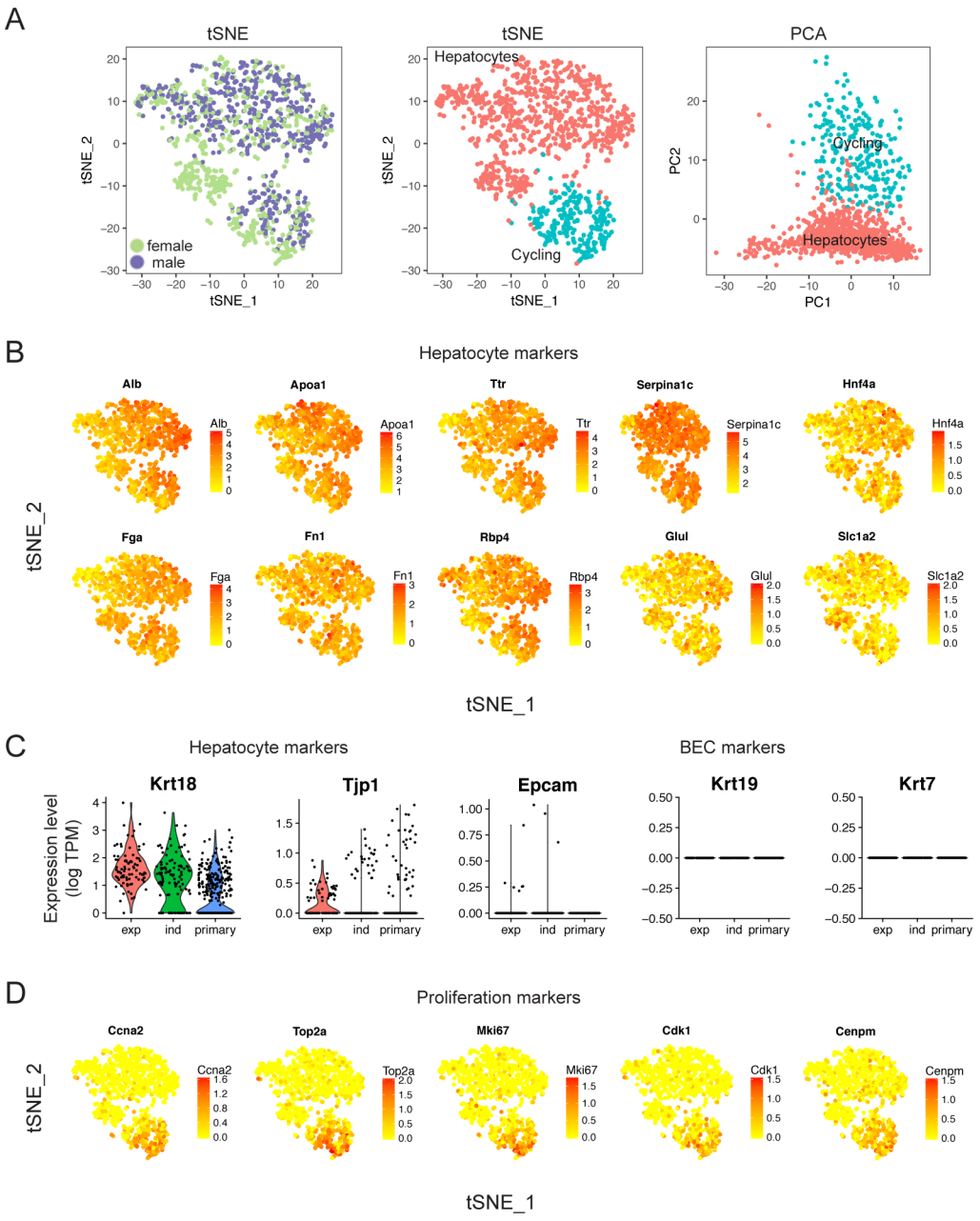

Figure 4. Single-cell RNA-seq reveals broad expression of hepatocyte markers and the presence of a subset of cycling cells.

(A)t-SNE projection of single cells (n = 1192) labeled by sex (left) or cycling state (middle) and the projection of the same cells onto the first two PCs (right).

(B)t-SNE plots indicating the (log-scale) expression of representative hepatocyte markers.

(C) Violin plots showing the (log-scale) expression of representative hepatocyte markers and the absence of biliary markers, '*exp*' = expansion, '*ind*' = induction and primary hepatocytes, n = subset of 100 cells shown.

(D) t-SNE plots indicating the (log-scale) expression of representative markers associated with proliferation.

.Related to Figure S5.

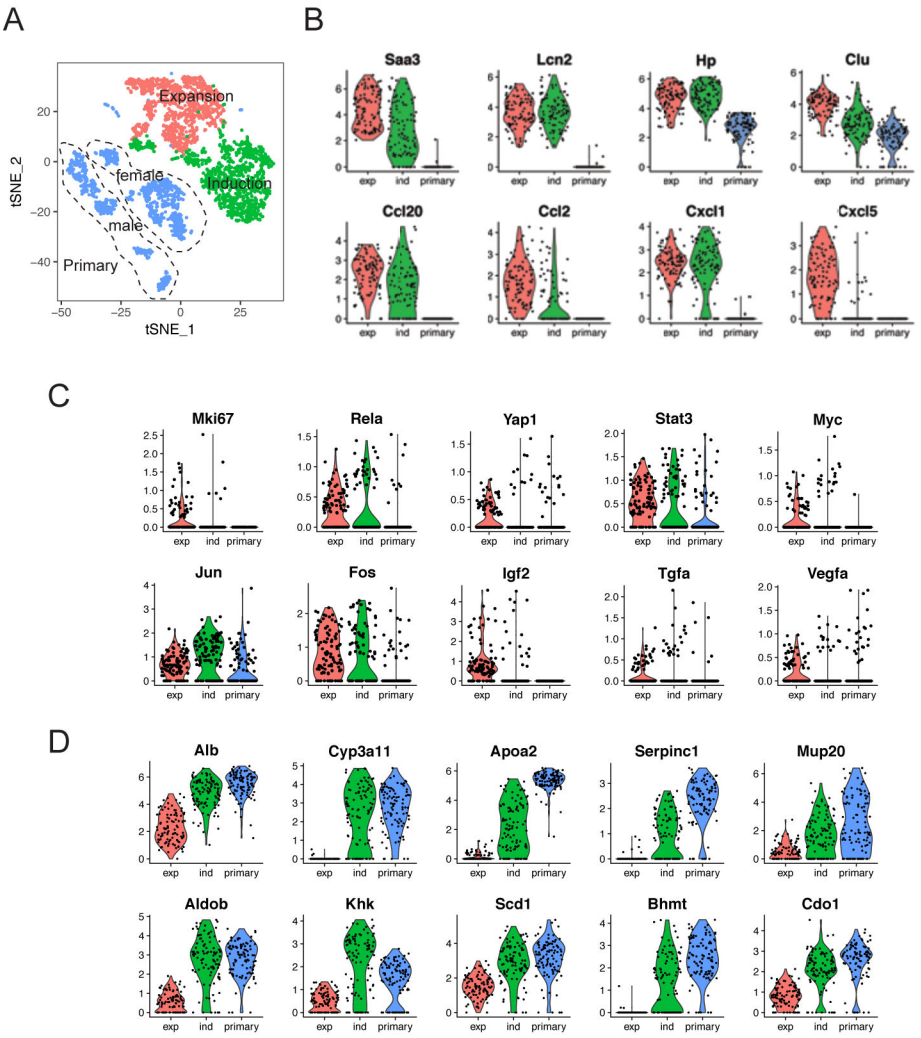

Figure 5. Expression of regeneration- associated markers in expanding media and upregulation of functional genes in induction media.

(A) t-SNE plot of 3D hepatocytes in expansion (*exp*) or induction (*ind*) media and primary hepatocytes.

(B) Violin plots of select top DEGs (log-scale) in *exp* hepatocytes relative to primary hepatocytes, with *ind* hepatocytes included for comparison. DEGs are determined by the top Wilcoxon rank sum test scores. Also shown in Figure S5A.

(C) Violin plots showing the (log-scale) expression of representative markers associated with liver regeneration.

(D) Violin plots showing the (log-scale) expression of selected upregulated genes in *ind* hepatocytes relative to *exp* hepatocytes, with primary hepatocytes included for comparison. Also shown in Figure S5B.

Related to Figure S5.

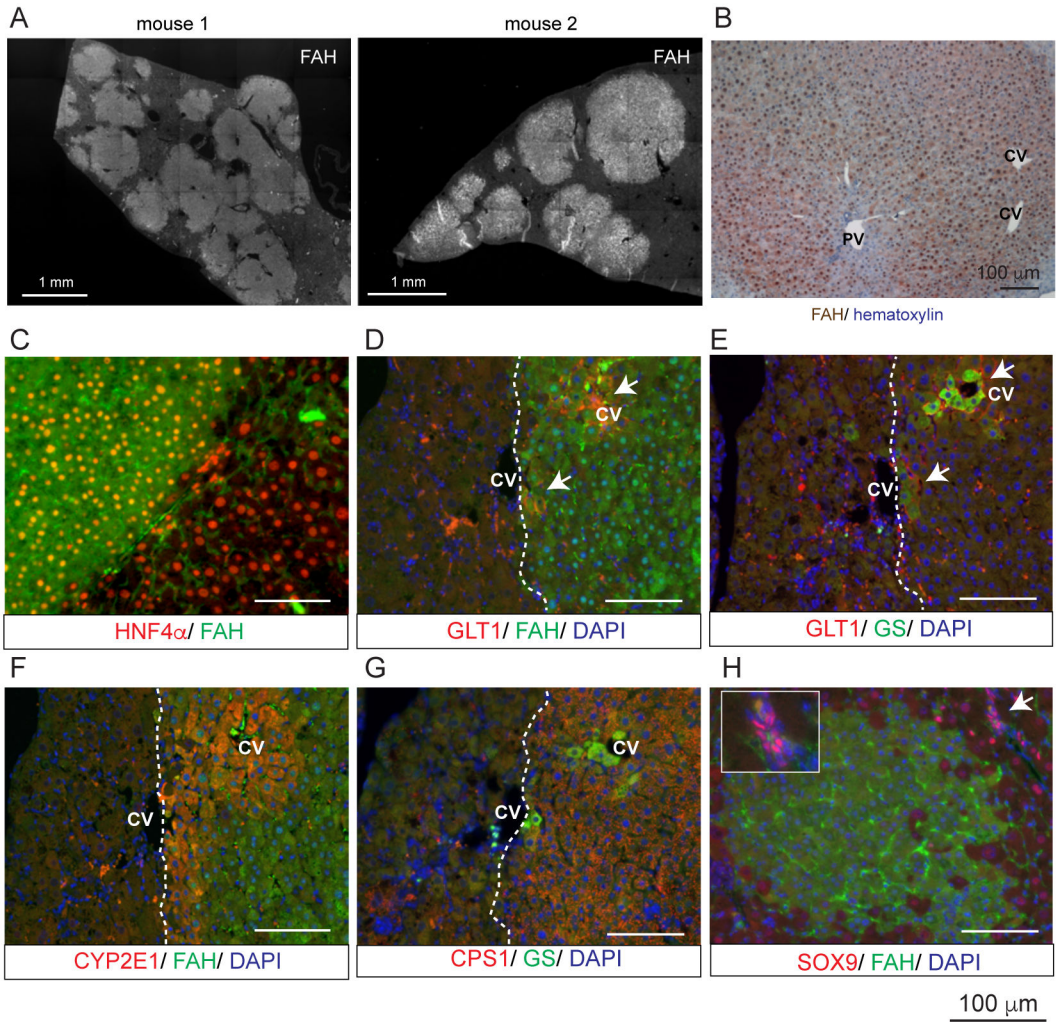

Figure 6. Cultured hepatocytes can engraft in Fah-deficient mice and express hepatocyte markers.

(A) Montage of entire liver sections stained with FAH antibody. Two biological samples are shown here. See Figure 6SA for additional biological replicates.

(B) Immunohistochemistry for FAH and hematoxylin showing a low-magnification view of engraftment of FAH+ hepatocytes into $FAH^{-/-}$ recipient livers.

(C) Immunofluorescence staining for FAH and the hepatocyte marker HNF4α.

(D-G) Immunofluorescence staining for various markers on serial sections. The dashed line demarcates the boundary between FAH+ and FAH− cells. Arrows mark membrane GLT1 staining.

(H) Immunofluorescence staining for FAH and the biliary marker SOX9 (arrow). Inset, a higher magnification of the bile duct. Scale bars = 100 μm, unless stated otherwise.

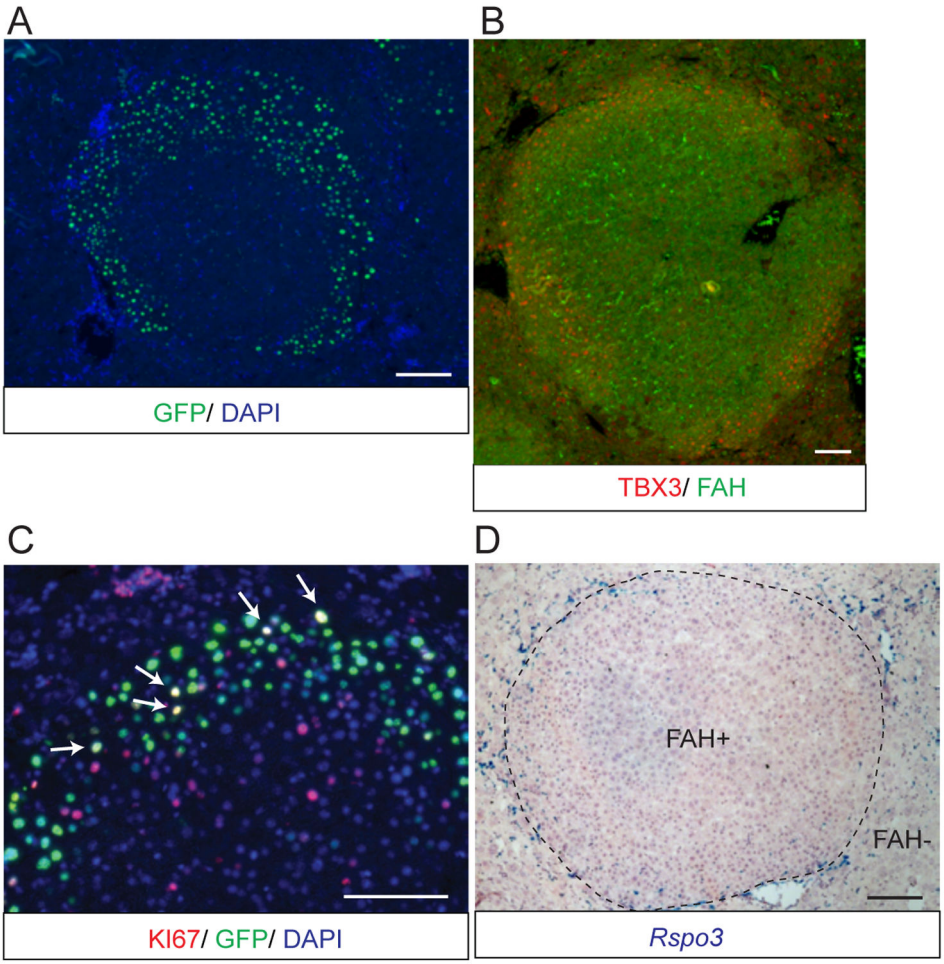

Figure 7. Active Wnt signaling at the FAH+ clone boundary.

(A) Wide-field image of an FAH liver section stained for GFP. Donor hepatocytes were derived from Axin2-rtTA;Tet-O-GFP mice (see Experimental Procedures).

(B) Overlay of immunofluorescence staining for TBX3 and FAH.

(C) Overlay of immunofluorescence staining for KI67 and GFP. Arrows mark nuclei that are double positive for both GFP and KI67.

(D) In situ hybridization for *Rspo3* counterstained with hematoxylin. Dashed line outlines the FAH clone boundary. Scale bars = 100 μm.

Table 1.

Taqman™ q-PCR probes.

Gene	Probe ID	Dye	Amplicon Length	Exon Coverage
Alb	Mm00802090_m1	FAM-MGB	89	14-15
Apoe	Mm01307193_g1	FAM-MGB	79	2-3
Cps1	Mm01256489_m1	FAM-MGB	69	36-37
Cyp1a2	Mm00487224_m1	FAM-MGB	73	3-4
Cyp2f2	Mm00484087_m1	FAM-MGB	88	4-5
Cyp3a11	Mm00731567_m1	FAM-MGB	128	10-11
Fah	Mm00487336_m1	FAM-MGB	65	1-2
Gck	Mm00439129_m1	FAM-MGB	69	7-8
Tat	Mm01244282_m1	FAM-MGB	61	10-11
Ttr	Mm00443267_m1	FAM-MGB	62	3-4

Table 2:

Antibodies

Antibody target	Vendor	Catalog #	species	Dilution
CD26	R&D	AF954	Goat	1:50
CPS1	Abcam	Ab3682	Mouse	1:50
CYP2E1	Abcam	ab28146	Rabbit	1:100
FAH	ABM	T123010	Mouse	1:100
FAH RABBIT	Produced in house in M. Grompe's lab		Rabbit	1:100
GLT1	Frontier Institute	Glt-1-Rb-Af670	Rabbit	1:100
GS	Millipore	MAB302	Mouse	1:500
HNF4α	Abcam	Ab41898	Mouse	1:50
HNF4α	Santa Cruz	Sc-8987	Rabbit	1:50
KI67	eBioscence	14-5698-82	Rat	1:100
SOX9	EMD Millipore	AB5535	Rabbit	1:200
YAP	Cell Signaling Technologies	4912S	Rabbit	1:100

KEY RESOURCES TABLE

REAGENT or RESOURCE	SOURCE	IDENTIFIER
Antibodies		
Rabbit Polyclonal anti-CPS1	Abcam	Cat# Ab3682; RRID:AB_304000
Rabbit Polyclonal anti- Cytochrome P450 2E1 (CYP2E1)	Abcam	Cat# Ab28146; RRID:AB_2089985
Goat Polyclonal anti-DPPIV/CD26	R&D systems	Cat# AF954; RRID:AB_355739
Mouse Monoclonal anti-FAA(FAH)	ABM	Cat# T123010 RRID: to be updated.
Rabbit Polyclonal anti-FAH	M Grompe's lab	Cat# OR026
Rabbit Polyclonal anti-GLT1	Frontier Institute	Cat# GLT1-Rb-Af670; RRID:AB_2571718
Mouse Monoclonal anti-GS (Clone GS-6)	Millipore	Cat#MAB302; RRID:AB_2110656
Rabbit Polyclonal anti- Hnf4α (Clone H-171)	Santa Cruz Biotechnology	Cat#SC-8987; RRID:AB_2116913
Mouse Monoclonal anti- Hnf4α (Clone K9218)	Abcam	Cat# Ab41898; RRID: AB_732976
Rat Monoclonal anti- Ki67 (SolA15)	eBioscience	Cat#14-5698-82; RRID: AB_10854564
Rabbit Polyclonal anti-KRT7 (CK7)	Millipore	Cat# HPA007272; RRID: AB_1079181
Rabbit anti-CK19 (KRT19)	AbboMax	Cat# 602-670; RRID:N/A
Rabbit polyclonal anti- NF-κB p65 (phospho S536)	Abcam	Cat#ab86299; RRID:AB_1925243
Rabbit Polyclonal anti- Sox9	Millipore	Cat# AB5535; RRID: AB_2239761
Goat Polyclonal anti-TBX3 (Clone A-20)	Santa Cruz Biotechnology	Cat#SC-17871; RRID:AB_661666
Rabbit polyclonal anti-YAP	Cell Signaling Technology	Cat#4912S; RRID:AB_2218911
Bacterial and Virus Strains		
Biological Samples		
Chemicals, Peptides, and Recombinant Proteins		
Liver Perfusion Medium (LP)	Invitrogen	17701-038
Collagenase type IV	Wellington	LS004188
HBSS with Ca Mg	GIBCO	24020117
100 μm strainer	Falcon	352360

REAGENT or RESOURCE	SOURCE	IDENTIFIER
24 gauge 3/4 inch angiocatheter	BD	381700
Percoll Plus	Sigma	E0414-250mL
Matrigel GF reduced	BD	356231
William E media	Gibco	A1217601
Glutamax	Gibco	35050-061
Non-Essential Amino Acids	Gibco	11140-050
Penicillin/streptomycin	Gibco	15140-122
Normocin	Invitrogen	ant-nr-2
B27	Gibco	17504-044
N2 supplement	Gibco	17502048
Nicotinamide	Sigma-Aldrich	N0636
N-acetylcysteine	Sigma-Aldrich	A9165
Y27632	Peprotech	1293823
A83-01	Tocris	2939
CHIR 99021	Peprotech	2520691
EGF	Peprotech	AF-100-15
HGF	Peprotech	100-39-100
TNFα	Peprotech	315-01A
Noggin	Peprotech	250-38
Dexamethasone	Tocris	1126
Dispase	Stem Cell Technologies	07913
IL-6	Thermo	Mm00446190_m1
TrypLE Express	Gibco	12605010
Bambanker	Wako	50-999-554
Luciferin-IPA	Promega	V9001
Fluorescein diacetate	Santa Cruz Biotechnology	sc-294598
Trypsin-EDTA solution	Gibco	25200056
DMEM	Thermo	11965092
HSC LipidTOX	Invitrogen	H34475

REAGENT or RESOURCE	SOURCE	IDENTIFIER
Reserpine	Sigma Aldrich	R0875-1G
Histogel	Thermo	22-110-678
Hoechst 33342	Life Technologies	H3570
Propidium iodide	Life Technologies	P1304MP
NTBC	Yecuris	20-0026
Critical Commercial Assays		
RNAscope 2.5 HD Reagent Kit-Red	Advanced Cell Diagnostics	Cat# 322360
RNAscope 2.5 HD Duplex Reagent Kit	Advanced Cell Diagnostics	Cat# 322430
RNeasy mini kit	Qiagen	74104
High Capacity cDNA Reverse Transcription kit	Life Technologies	4368814
mouse albumin ELISA kit	Assaypro	EMA2201-1
LDL Uptake Assay Kit	Abcam	ab1331267
Periodic Acid-Schiff kit	Sigma Aldrich	395B-1KT
Deposited Data		
10x single-cell RNA seq dataset	This paper	To be deposited.
Experimental Models: Cell Lines		
HEK293T	ATCC	CRL-1573
GFP expressing human umbilical vein endothelial cells(GFP-HUVECs)	Angioproteomie	cAP-0001GFP
Experimental Models: Organisms/Strains		
C57BL/6J	Jackson lab	000664
Axin2-CreERT2	Jackson lab	018867
Axin2-rtTA	Jackson lab	016997
Rosa26-mTmG	Jackson lab	007676
TetO-H2B:GFP	Jackson lab	005104
Oligonucleotides		

REAGENT or RESOURCE	SOURCE	IDENTIFIER
RNAscope Probe: Mm-Fah-C2 (target region: 490-1364)	Advanced Cell Diagnostics	Cat#503431-C2
RNAscope Probe: Mm-Wnt9b (target region: 706-1637)	Advanced Cell Diagnostics	Cat#405091
RNAscope Probe: Mm-Wnt2 (target region: 857-2086)	Advanced Cell Diagnostics	Cat#313601
RNAscope Probe: Mm-Rspo3 (target region: 731-2164)	Advanced Cell Diagnostics	Cat#402011
RNAscope Probe: Mm-Rspo 1 (target region: 550-1679)	Advanced Cell Diagnostics	Cat#401991
RNAscope Probe: Mm-Rspo2 (target region: 537-1452)	Advanced Cell Diagnostics	Cat# 402001
RNAscope Probe: Mm-Rspo4 (target region: 1180-2202)	Advanced Cell Diagnostics	Cat#402021
RNAscope Probe: Mm-CD31/Pecam1-C2 (target region: 915-1827)	Advanced Cell Diagnostics	Cat#316721-C2
RNAscope Probe: Mm-CD45/Ptprc-C2 (target region: 2922-3866)	Advanced Cell Diagnostics	Cat# 318651-C2
RNAscope Probe: Mm-TNFa (target region: 41-1587)	Advanced Cell Diagnostics	Cat# 311081
Taqman Probe Alb	Applied Biosystem	Cat# 4331182 Mm00802090_m1
Taqman Probe Apoe	Applied Biosystem	Cat# 4331182 Mm01307193_g1
Taqman Probe: Cps1	Applied Biosystem	Cat# 4331182 Mm01256489_m1
Taqman Probe: Cyp1a2	Applied Biosystem	Cat# 4331182 Mm00487224_m1
Taqman Probe: Cyp2f2	Applied Biosystem	Cat# 4331182 Mm00484087_m1
Taqman Probe: Cyp3a11	Applied Biosystem	Cat# 4331182 Mm00731567_m1
Taqman Probe: Fah	Applied Biosystem	Cat# 4331182 Mm00487336_m1
Taqman Probe: Gck	Applied Biosystem	Cat# 4331182 Mm00439129_m1
Taqman Probe: Tat	Applied Biosystem	Cat# 4331182 Mm01244282_m1

REAGENT or RESOURCE	SOURCE	IDENTIFIER
Taqman Probe: Ttr	Applied Biosystem	Cat# 4331182 Mm00443267_m1
Recombinant DNA		
Plasmid :1-puro-CMV-TurboGFP	Sigma Aldrich	SHC003
Plasmid: psPAX2	Addgene	12260
Plasmid: pMD.2g	Addgene	12259
Software and Algorithms		
Prism Graphpad 7.0	Graphpad software	http://www.graphpad.com
Adobe Photoshop CC 2018	Adobe	http://www.adobe.com/product/photoshop.html
Adobe Illustrator CC 2018	Adobe	http://www.adobe.com/product/illustrator.html
Image J	NIH	http://imagej.nih.gov/ij/
Cell Ranger version 2.1.1	10x Genomics	https://support.10xgenomics.com/single-cell-gene-expression/sof
Seurat R Package	Butler et al., 2018	https://satijalab.org/seurat
HCS Studio Cell Analysis Software	Thermo Fisher	https://thermofisher.com
Other		